Inorganic Chemistry

Article

pubs.acs.org/IC

# Experimental and Theoretical Investigations of Magnetic Exchange Pathways in Structurally Diverse Iron(III) Schiff-Base Complexes

Radovan Herchel, Ivan Nemec, Marek Machata, and Zdeněk Trávníček*

Regional Centre of Advanced Technologies and Materials, Department of Inorganic Chemistry, Faculty of Science, Palacký University, 17. listopadu 12, CZ-771 46 Olomouc, Czech Republic

Supporting Information

**ABSTRACT:** The synthesis, and the structural and magnetic properties, of the following new iron(III) Schiff base complexes with the {O′,N,O″}-chelating ligand $H_2L$ (2-hydroxyphenylsalicylaldimine) are reported: $K[FeL_2]\cdot H_2O$ (**1**), $(Pr_3NH)[FeL_2]\cdot 2CH_3OH$ (**2**), $[FeL(bpyO_2)(CH_3OH)][FeL_2]\cdot CH_3OH$ (**3**), $[Fe_2L_3(CH_3OH)]\cdot 2CH_3OH\cdot H_2O$ (**4**), and $[\{Fe_2L_2\}(\mu\text{-}OH)_2\{FeL(bpyO_2)\}_2][BPh_4]_2\cdot 2H_2O$ (**5**), where $Pr_3NH^+$ represents the tripropylammonium cation and $bpyO_2$ stands for 2,2′-bipyridine-*N*-dioxide. A thorough density functional theory (DFT) study of magnetic interactions (the isotropic exchange) at the B3LYP/def-TZVP level of theory was employed, and calculations have revealed superexchange pathways through intramolecular/intermolecular noncovalent contacts ($\pi-\pi$ stacking, C−H···O and O−H···O hydrogen bonds, diamagnetic metal cations) and/or covalent bonds (($\mu$-$O_{Ph}$, $\mu$-OH) or bis($\mu$-$O_{Ph}$) bridging modes), which helped us to postulate trustworthy spin Hamiltonians for magnetic analysis of experimental data. Within the reported family of compounds **1**−**5**, the mediators of the antiferromagnetic exchange can be sorted by their increasing strength as follows: $\pi-\pi$ stacking ($J^{DFT}$ = −0.022 $cm^{-1}$/$J^{mag}$ = −0.025(4) $cm^{-1}$ in **2**) < C−H···O contacts and $\pi-\pi$ stacking ($J^{DFT}$ = −0.19 $cm^{-1}$/$J^{mag}$ = −0.347(9)$cm^{-1}$ in **1**) < O−H···O hydrogen bonds ($J^{DFT}$ = −0.53 $cm^{-1}$/$J^{mag}$ = −0.41(1) $cm^{-1}$ in **3**) < bis($\mu$-$O_{Ph}$) bridge ($J^{DFT}$ = −13.8 $cm^{-1}$/$J^{mag}$ = −12.3(9) $cm^{-1}$ in **4**) < ($\mu$-$O_{Ph}$, $\mu$-OH) bridge ($J^{DFT}$ = −18.0 $cm^{-1}$/$J^{mag}$ = −17.1(2) $cm^{-1}$ in **5**), where $J^{DFT}$ and $J^{mag}$ are the isotropic exchange parameters derived from DFT calculations, and analysis of the experimental magnetic data, respectively. The good agreement between theoretically calculated and experimentally derived isotropic exchange parameters suggests that this procedure is applicable also for other chemical and structural systems to interpret magnetic data properly.

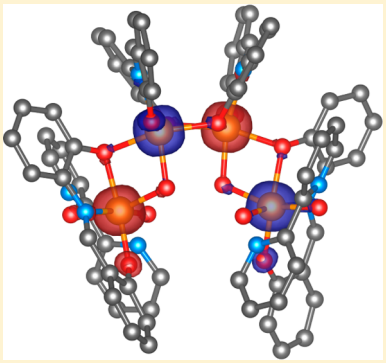

## INTRODUCTION

Extracting information about magnetic interactions in coordination compounds from experimental data is still a complex task that requires knowledge of the crystal structure, an adequate acquisition of magnetic data, and a properly proposed theoretical model. Within the spin Hamiltonian formalism, the spin−spin magnetic interaction[1] is most commonly described by the isotropic exchange, eventually accompanied by non-isotropic terms (the zero-field splitting,[2] the asymmetric exchange,[3] or the antisymmetric exchange[4]). The determination of these intrinsic parameters and their relation to the molecular or even crystal structure is the key to provide basic tools for rational design of molecular materials with extraordinary magnetic properties. Unquestionably, single-molecule magnets (SMMs)[5] belong into this class of magnetic materials, and, despite the fact that, in most polynuclear iron(III) complexes, the antiferromagnetic exchange interactions between Fe centers dominates,[6] some of them possess a large spin ground state, coupled with a significant easy axis magnetic anisotropy resulting in SMM behavior.[7] Furthermore, precise knowledge about the electronic and magnetic properties is crucial in the field of bioinorganic chemistry, where mainly $\mu$-hydroxo-, $\mu$-oxo-, and $\mu$-carboxylate-bridged iron complexes represent synthetic models of the active sites of various nonheme iron proteins, such as hemerythrin, ribonucleotide reductase, methane monooxygenase, and fatty acyl desaturases, which contain diiron cores bridged by the above-mentioned moieties.[8]

However, the complexity of magnetic interactions in polynuclear complexes and/or the intricacy of intermolecular interactions in the solid state are tackled with difficulties when only temperature-dependent data (susceptibility) are treated. Thus, either more-sophisticated experimental techniques (e.g., inelastic neutron scattering, tunable-frequency high-field electron paramagnetic resonance (EPR)) or *ab initio* theoretical approaches such as density function methods (DFT) enable us to address the behaviors of transition-metal complexes properly.[9] The magnetic properties of studied complexes are usually analyzed by models based on long-term experience and knowledge of the literature data, where covalent interactions dominate. However, with technological progress in experimental instrumentation designed for measurements of magnetic data, the amount of information increases and enables us to determine also minor or weak magnetic interactions within coordination compounds.

**Received:** June 5, 2015
**Published:** August 11, 2015





DOI: 10.1021/acs.inorgchem.5b01271
*Inorg. Chem.* 2015, 54, 8625−8638

Herein, the importance of *ab initio* theoretical methods emerges, and, in our opinion, the mutual cooperation between the conventional magnetic analysis (the spin Hamiltonian model proposal, fitting experimental data) and theoretical calculation of the spin Hamiltonian parameters based on molecular/crystal structure is inevitable. Usually, the theoretical calculations are used to support the analysis of experimental magnetic data; however, because of the great progress in computational chemistry software and hardware, we suggest screening all potential superexchange pathways, found from the analysis of the molecular/crystal structure, by advanced *ab initio* methods (e.g., DFT) and using them to postulate trustworthy spin Hamiltonians to analyze the experimental data (see Scheme 1).

**Scheme 1. (Left) Suggested methodology, where *ab initio* calculations have a predictive role. (Right) Most-used approach, where *ab initio* calculations eventually serve to support magnetic analysis**

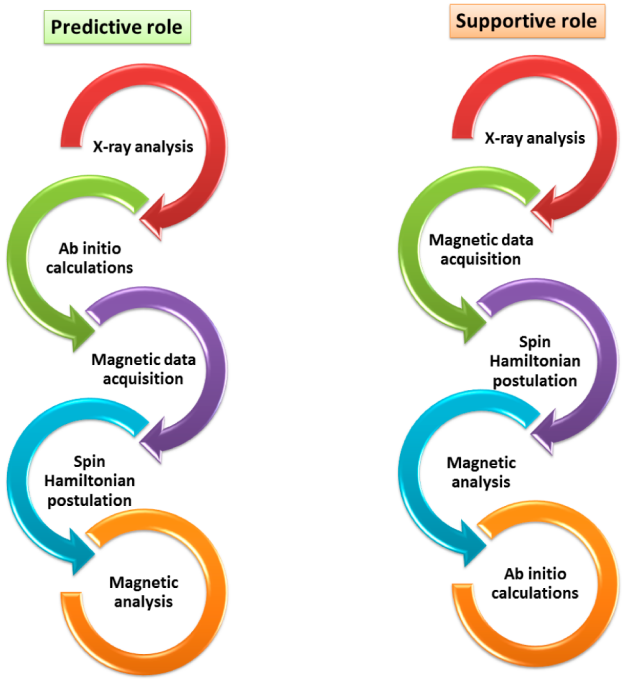


To defend this opinion, herein, we present the thorough analysis of magnetic properties of the newly prepared family of mononuclear $K[FeL_2]\cdot H_2O$ (**1**), $Pr_3NH[FeL_2]\cdot 2CH_3OH$ (**2**), and polynuclear $[FeL(bpyO_2)(CH_3OH)][FeL_2]\cdot CH_3OH$ (**3**), $[Fe_2L_3(CH_3OH)]\cdot 2CH_3OH\cdot H_2O$ (**4**), $[\{Fe_2L_2\}(\mu\text{-}OH)_2\{FeL(bpyO_2)\}_2][BPh_4]_2\cdot 2H_2O$ (**5**) iron(III) coordination compounds utilizing tridentate Schiff base {O′,N,O″} chelating ligand $H_2L$ (2-hydroxyphenylsalicylaldimine), where $Pr_3NH^+$ is tripropylammonium cation and $bpyO_2$ is 2,2′-bipyridine-*N*-dioxide. Herein, the reported family of Fe(III) complexes gave us an opportunity to scrutinize, in detail, the limits of magnetochemical analysis and DFT-based theoretical methods to assess magnetic exchange through $\pi$–$\pi$ stacking, intramolecular and intermolecular hydrogen bonds, diamagnetic metal cations, and coordinate covalent bonds. Thus, the advantages and limits of both spin Hamiltonian formalism applied to experimental temperature/field-dependent magnetization data and theoretical treatment using DFT calculations at B3LYP/def2-TZVP level of theory are discussed in detail.

## EXPERIMENTAL SECTION

**Chemicals and Physical Methods.** All chemicals purchased were chemically pure and of analytical reagent grade, and were used without further purification. Elemental analyses (C, H, N) were performed on a FLASH 2000 CHNS Analyzer (ThermoFisher Scientific). Infrared spectra of the complexes were recorded on a ThermoNicolet NEXUS 670 FT-IR spectrometer, using the attenuated total reflectance (ATR) technique in the range of 400−4000 $cm^{-1}$. The temperature-dependent ($T$ = 1.9−300 K, $B$ = 0.1 T) and field-dependent ($B$ = 0−7 T, $T$ = 2 and 4.6 or 5 K) magnetization measurements were performed on polycrystalline samples with an MPMS XL-7 Quantum Design SQUID magnetometer. Experimental data were corrected for the diamagnetism of the constituent atoms.

**Synthesis of $K[FeL_2]\cdot H_2O$ (1) and $Pr_3NH[FeL_2]$ (2).** An orange mixture of salicylaldehyde (1.22 g, 10 mmol) and 2-aminophenol (1.09 g, 10 mmol) in 25 $cm^3$ of methanol was stirred at laboratory temperature for 15 min. Addition of methanolic solution (15 $cm^3$) of $FeCl_3\cdot 6H_2O$ (1.37 g, 5 mmol) changed the color to dark red. After 15 min, a methanolic solution of a base (1.12 g, 20 mmol of KOH (**1**) or 2.86 g, 20 mmol of $Pr_3N$ (**2**) in 5 $cm^3$ of methanol) was added dropwise and the resulting mixture was stirred under reflux for next 15 min, and then filtered through the paper filter. Black prism shaped crystals of **1** and **2** were obtained by slow evaporation of the mother liquor after 2 days and they were collected by filtration and washed by methanol and diethyl ether, and dried in the open air. Anal. Calcd for **1** ($C_{26}H_{20}FeKN_2O_5$, $M_r$ = 535.4): C, 58.3; H, 3.8; N, 5.2. Found: C, 57.9; H, 3.6; N, 5.0. $\Lambda_M$ (DMF, $10^{-4}$ S $cm^2$ $mol^{-1}$) = 65.25. FT-IR mid (in $cm^{-1}$): $\nu$(O−H) = 3305 (w), $\nu$(N−H) = 3189 (w), $\nu(C-H)_{aromatic}$ = 3050 (w), $\nu$(C═N) and $\nu$(C═C) = 1599, 1580, 1535 (vs). Anal. Calcd for **2** ($C_{35}H_{40}FeN_3O_4$, $M_r$ = 622.6): C, 67.5; H, 6.5; N, 6.8. Found: C, 67.8; H, 6.8; N, 7.0. FT-IR mid (in $cm^{-1}$): $\nu(C-H)_{aromatic}$ = 3054 (w), $\nu(C-H)_{aliphatic}$ = 3008, 2963, 2930, 2872 (m), $\nu$(C═N) and $\nu$(C═C) = 1600, 1580, 1531 (vs).

**$[Fe(bpyO_2)(L)(H_2O)]Cl$ (3′).** A brown mixture of $bpyO_2$ (0.941 g, 5 mmol), $H_2L$ (1.07 g, 5 mmol) and $FeCl_3\cdot 6H_2O$ (1.35 g, 5 mmol) in 40 $cm^3$ methanol was stirred at boiling point of the solution for 20 min. Then $Pr_3N$ (1.43 g, 10 mmol) was slowly added and the resultant mixture was heated for 15 min. A brown precipitate was filtered off and the mother liquor was left unperturbed for slow evaporation of the solvent. After 1 day, brownish microcrystals were collected by filtration and washed by methanol and diethyl ether and dried in the open air. Since we were not successful in the preparation of single crystals for X-ray diffraction analysis, the composition of this compound was determined using the results of elemental analysis and molar conductivity (comparison with **1**). As a result, we suppose that the chlorido ligand is not bound to the Fe atom. Anal. Calcd for **3′** ($C_{23}H_{19}FeN_3O_5Cl$, $M_r$ = 508.7): C, 54.3; H, 3,8; N, 8.3. Found: C, 54.6; H, 3.8; N, 8.1. $\Lambda_M$ (DMF, $10^{-4}$ S $cm^2$ $mol^{-1}$) = 70.75. FT-IR mid (in $cm^{-1}$): $\nu$(O−H) = 3230 (w), $\nu(C-H)_{aromatic}$ = 3046 (w), $\nu(C-H)_{aliphatic}$ = 2965, 2584, 2607 (m), $\nu$(C═N) and $\nu$(C═C) = 1600, 1582, 1535 (vs).

**Synthesis of $[FeL(bpyO_2)(CH_3OH)][FeL_2]\cdot CH_3OH$ (3).** Complex **2** (0.311 g, 0.5 mmol) and the equivalent amount of complex **3′** (0.254 g, 0.5 mmol) were suspended together in 50 $cm^3$ of methanol and they were stirred at 50 °C for 30 min. The mixture was filtered and the mother liquor was left undisturbed. After 2 days, the crystalline product was formed and prism-shaped crystals were collected by filtration and washed by methanol and diethyl ether and dried in open air. Anal. Calcd for **3** ($C_{51}H_{43}Fe_2N_5O_{10}$, $M_r$ = 997.6): C, 61.4; H, 4.3; N, 7.0. Found: C, 61.2; H, 4.3; N, 7.1. FT-IR mid (in $cm^{-1}$): $\nu$(O−H) = 3540 (w), $\nu(C-H)_{aromatic}$ = 3084, 3053, 3023 (w), $\nu(C-H)_{aliphatic}$ = 2965, 2584, 2607 (m), $\nu$(C═N) and $\nu$(C═C) = 1602, 1583, 1535 (vs).

**Synthesis of $[Fe_2L_3(CH_3OH)]\cdot 2CH_3OH\cdot H_2O$ (4).** This compound was prepared as described for **2**, but a different molar ratio of the reagents was used−salicylaldehyde (0.057 g, 0.469 mmol), 2-aminophenol (0.051 g, 0.46 mmol), $FeCl_3\cdot 6H_2O$ (0.084 g, 0.313 mmol) and $Pr_3N$ (0.134 g, 0.940 mmol). Anal. Calcd for **4** ($C_{42}H_{41}Fe_2N_3O_{10}$, $M_r$ = 859.5): C, 58.7; H, 4.8; N, 4.9. Found: C,


DOI: 10.1021/acs.inorgchem.5b01271
*Inorg. Chem.* 2015, 54, 8625−8638

Table 1. Crystal Data and Structure Refinements for Compounds 1−5[a]

| | 1 | 2 | 3 | 4 | 5 |
|---|---|---|---|---|---|
| formula | $C_{26}H_{20}FeKN_2O_5$ | $C_{35}H_{40}FeN_3O_4$ | $C_{51}H_{43}Fe_2N_5O_{10}$ | $C_{42}H_{41}Fe_2N_3O_{10}$ | $C_{120}H_{98}B_2Fe_4N_8O_{15}$ |
| formula weight (g mol$^{-1}$) | 535.39 | 622.55 | 997.60 | 859.49 | 2137.08 |
| crystal color | brown | brown | brown | brown | brown |
| temperature (K) | 293(2) | 150(2) | 100(2) | 100(2) | 90(2) |
| wavelength (Å) | 0.71073 | 0.71073 | 0.71073 | 0.71073 | 0.71073 |
| crystal system | monoclinic | monoclinic | monoclinic | monoclinic | Triclinic |
| space group | $P2_1/c$ | $P2_1/c$ | $P2_1/c$ | $P2_1/c$ | $P$-1 |
| $a$ (Å) | 12.4940(6) | 9.2609(3) | 12.9916(3) | 15.9573(13) | 16.5387(5) |
| $b$ (Å) | 17.8349(9) | 25.8855(10) | 20.2079(6) | 16.0720(9) | 17.7318(6) |
| $c$ (Å) | 10.0392(6) | 12.9410(5) | 20.0079(6) | 16.0759(10) | 18.5063(6) |
| $\alpha$ (°) | 90 | 90 | 90 | 90 | 94.2800(10) |
| $\beta$ (°) | 93.817(5) | 92.822(3) | 124.567(2) | 16.0759(10) | 105.1800(10) |
| $\gamma$ (°) | 90 | 90 | 90 | 90 | 103.2240(10) |
| $V$ (Å$^3$) | 2232.1(2) | 3098.5(2) | 4325.4(2) | 3890.2(5) | 5046.4(3) |
| $Z$ | 4 | 4 | 4 | 4 | 2 |
| $\rho_{calc}$ (g cm$^{-3}$) | 1.593 | 1.335 | 1.532 | 1.467 | 1.406 |
| $\mu$ (mm$^{-1}$) | 0.906 | 0.530 | 0.741 | 0.809 | 0.636 |
| $F$(000) | 1100 | 1316 | 2064 | 1784 | 2216 |
| final $R$ indices | $R_1$ = 0.0392 | $R_1$ = 0.0471 | $R_1$ = 0.0377 | $R_1$ = 0.0380 | $R_1$ = 0.0323 |
| $[I > 2\sigma(I)]$ | $wR_2$ = 0.1018 | $wR_2$ = 0.1162 | $wR_2$ = 0.0838 | $wR_2$ = 0.0939 | $wR_2$ = 0.0766 |
| $R$ indices (all data) | $R_1$= 0.0596 | $R_1$= 0.0739 | $R_1$ = 0.0642 | $R_1$ = 0.0591 | $R_1$ = 0.0540 |
| | $wR_2$ = 0.1196 | $wR_2$ = 0.1221 | $wR_2$ = 0.0878 | $wR_2$ = 0.0991 | $wR_2$ = 0.0869 |
| GoF on $F^2$ | 1.107 | 1.043 | 0.944 | 0.954 | 1.022 |
| largest peak and hole (e Å$^{-3}$) | 0.416, −0.415 | 0.509, −0.274 | 0.653, −0.447 | 0.890, −0.537 | 0.491, −0.461 |
| CCDC Nos. | 1404952 | 1404953 | 1404954 | 1404955 | 1404956 |

[a]Crystallographic data available in the Supporting Information.

58.4; H, 4.7; N, 4.8. FT-IR mid (in cm$^{-1}$): $\nu$(O−H) = 3658 (w), 3344 (m), $\nu$(C−H)$_{aromatic}$ = 3063, 3020, 3023 (m), $\nu$(C═N) and $\nu$(C═C) = 1602, 1579, 1536 (vs).

**Synthesis of [{$Fe_2L_2$}($\mu$−OH)$_2${FeL(bpyO$_2$)}$_2$][$BPh_4$]$_2$·2$H_2O$ (5).** The [Fe(L)(bpyO$_2$)(CH$_3$OH)]Cl[10] complex (0.4 g, 0.765 mmol) was dissolved in 60 cm$^3$ of methanol and 4,4′-bipyridyl (0.068 g, 0.435 mmol) was added to this solution during its stirring. The brown solution was stirred and refluxed for 2 h after which it was filtered through a paper filter to a solution of $NaBPh_4$ (0.3 g, 0.877 mmol) in 10 cm$^3$ of methanol. The brown precipitate then was filtered off and the mother liquor was left to crystallize for several days and the microcrystalline powder was obtained. Single crystals of a sufficient quality were obtained by recrystallization of the microcrystalline powder from acetonitrile. Anal. Calcd for **5** ($C_{120}H_{98}B_2Fe_4N_8O_{16}$, $M_r$ = 2153.1): C, 66.9; H, 4.6; N, 5.2, Found: C, 66.7; H, 4.4; N, 5.1. FT-IR mid (in cm$^{-1}$): $\nu$(O−H) = 3485 (m), $\nu$(C−H)$_{aromatic}$ = 3061, 3027, 3028 (m), $\nu$(C═N) and $\nu$(C═C) = 1603, 1571, 1538 (vs), $\nu$(Ar−H)$_{BPh4}$ = 705.

**Single-Crystal X-ray Analysis.** X-ray measurements on the selected crystals of **1**−**4** were performed on an Oxford Diffraction Xcalibur$^2$ equipped with a Sapphire2 CCD detector using the Mo K$\alpha$ radiation. The CrysAlis program package (version 1.171.33.52, Oxford Diffraction) was used for data collection and reduction.[11] X-ray measurements on the selected crystal of **5** were performed on a Bruker SMART APEX-II diffractometer equipped with a rotating anode. Data collection, reduction, and absorption correction were performed using Bruker AXS software.[12] The molecular structures were solved by direct methods SHELX-97 and all non-hydrogen atoms were refined anisotropically on $F^2$ using full-matrix least-squares procedure SHELXL-97.[13] All hydrogen atoms were found in differential Fourier maps, and their parameters were refined using the riding model with $U_{iso}$(H) = 1.2 or 1.5 $U_{eq}$ (the atom of attachment). Nonroutine aspects of the structure refinement are as follows: in compounds **1**−**4**, the disorder of the imino moiety over two positions is observed. The disorder was modeled involving constraints of the anisotropic displacement parameters and with occupation factors as follows: **1**, C20A/B and N2A/B (A:B = 0.71:0.29); **2**, C7A/B and N1A/B (A:B = 0.63:0.37), C20A/B and N2A/B (A:B = 0.64:0.36); **3**, C33A/B and N3A/B (A:B = 0.74:0.26); and **4**, C7A/B and N1A/B (A:B = 0.85:0.15).

**Theoretical Methods.** The theoretical calculations were carried out with the ORCA 3.0.1 computational package.[14] The hybrid B3LYP functional[15] was used for the calculations of the isotropic exchange constants $J$, following Ruiz's approach,[16] by comparing the energies of high-spin (HS) and broken-symmetry spin (BS) states. The polarized triple-$\zeta$ quality basis set (def2-TZVP) proposed by Ahlrichs and co-workers was used for all atoms.[17] The calculations utilized the RI approximation with the decontracted auxiliary def2-TZVP/J Coulomb fitting basis sets and the chain-of-spheres (RIJCOSX) approximation to exact exchange as implemented in ORCA.[18] Increased integration grids (Grid4 in ORCA convention) and tight SCF convergence criteria were used in all calculations. In all of the cases, the calculations were based on the experimentally determined X-ray structures, but the positions of the hydrogen atoms were optimized using the B3LYP functional and atom-pairwise dispersion correction to the DFT energy with Becke-Johnson damping (D3BJ),[19] when these atoms were involved in the magnetic coupling path. The spin densities were visualized with the program VESTA 3.[20]

## RESULTS AND DISCUSSION

**General Overview.** The Schiff base ligands proved great potential utilized in the preparation of mononuclear and polynuclear complexes. Their versatility can be manifested by mentioning at least a few polynuclear iron(III) complexes prepared with polydentate chelating Schiff base ligands, such as salicylaldehyde oxime,[21] *N*-salicylidene-2-ethanolamine,[22] *N*,*N*′-bis(salicylidene)-*o*-phenylenediamine,[23] *N*,*N*′-bis(salicylidene)-1,3-diaminopropane[24] or substituted salicylideneamino alcohols.[5g] Some of these homovalent iron(III) compounds show slow relaxation of magnetization below the critical temperature (hence, SMM behavior).[5g,22a,f]



DOI: 10.1021/acs.inorgchem.5b01271
Inorg. Chem. 2015, 54, 8625−8638

To date, the complexes of iron(III) and tridentate {O′,N,O″} Schiff base chelating ligand $H_2L$ (2-hydroxyphenylsalicylaldimine) and its close derivatives were reported to be basically homoleptic or heteroleptic mononuclear,[25] dinuclear,[26] or trinuclear,[25b] depending on iron-to-ligand (Fe:L) ratio found in the complex. The dianionic and tridentate ligand $L^{2-}$ provides $N_2O$ donor set and coordinates through one N atom from imino group and two phenolate O atoms, and these phenolate groups can form bridges in polynuclear complexes. In the case of homoleptic complex anions $[FeL_2]^-$, the resultant chromophore $\{FeN_2O_4\}$ is not able to accommodate ligand-field strength to stabilize the low-spin state of the central iron(III) atom; therefore, such complexes are high spin (HS) ($S = 5/2$, $^6A_{1g}$ in octahedral geometry). Actually, the only low-spin (LS) Fe(III) complex involving the $L^{2-}$ ligand is $(PPh_4)_2[FeL(CN)_3]$ (where $PPh_4^+$ is the tetraphenylphosphonium cation), where the strong ligand field is induced by the cyanido ligands.[27] Other mononuclear and polynuclear heteroleptic complexes are reported as the HS complexes in which the bridging between the Fe(III) centers is provided by the phenoxy O atoms from the $L^{2-}$ ligands and the magnetic exchange interactions are reported as antiferromagnetic.[26c] Only very recently, the 3-methoxy-substituted ($H_2$3MeO-L) derivative of the $H_2L$ ligand was used for the preparation of heterobimetallic 3*d*-4*f* complexes: tetranuclear $Ni_2Ln_2$,[28] hexanuclear $Ni_4Ln_2$,[29] and trinuclear $Fe_2Ln$.[25d] In the case of $Fe_2Ln$ complexes, solely ferromagnetic interactions between the Fe(III) and 4f atoms were observed.

Herein, we report on the preparation of mononuclear iron(III) precursors $K[FeL_2]\cdot H_2O$ (**1**) and $Pr_3NH[FeL_2]\cdot 2CH_3OH$ (**2**), and polynuclear iron(III) complexes $[FeL(bpyO_2)(CH_3OH)][FeL_2]\cdot CH_3OH$ (**3**), $[Fe_2L_3(CH_3OH)]\cdot 2CH_3OH\cdot H_2O$ (**4**), $[\{Fe_2L_2\}(\mu\text{-}OH)_2\{FeL(bpyO_2)\}_2][BPh_4]_2\cdot 2H_2O$ (**5**), where $Pr_3NH^+$ represents the tripropylammonium cation and $bpyO_2$ stands for 2,2′-bipyridine-*N*-dioxide. For the reported compounds, we present synthesis, structural, and magnetic properties. The magnetic analysis was performed experimentally and theoretically using a SQUID magnetometer and DFT calculations at the B3LYP/def2-TZVP level of theory, respectively.

The crystallographic data for compounds **1**−**5** are reported in Table 1, and bond lengths typical for the Fe(III) complexes with $H_2L$ and its derivatives (further labeled as $H_2$R-L, where R marks a substituent on the aromatic ring of the salicylaldiminato moiety) are summarized in Table 2. Bond lengths between the Fe(III) atom and phenolate O atoms ($Fe-O_{Ph}$) are within a relatively narrow range: 1.93−2.00 Å, while the imino nitrogen ($N_{im}$) with Fe(III) atoms form bonds more variable in length: $Fe-N_{im}$ = 2.06−2.20 Å. From the values of the angular distortions from the ideal octahedron ($\Sigma$),[30] it is apparent that their values are significantly higher when the R-$L^{2-}$ ligand is involved in bridging between the Fe(III) atoms.

Concerning theoretical calculations of the spin Hamiltonian parameters by *ab initio* methods, there have been great efforts devoted to the development of various theoretical methods to calculate the isotropic and even anisotropic exchange parameters in molecular systems, containing unpaired electrons in *p*, *d*, or *f* orbitals.[31] The most employed method seems to be DFT, where various types of functionals were developed.[32] The most popular approach used to calculate the isotropic exchange in molecular system seems to be based on comparison of energies of high-spin (HS) state and so-called the broken-symmetry spin (BS) state, where, however, the problem of spin contamination also must be treated by various ways.[9] Herein, we used Ruiz's approach,[16] because it can be also easily utilized to polynuclear systems.[33]

**Table 2. Selected Structural Parameters for Iron(III) Complexes Involving 2-Hydroxyphenylsalicylaldimine ($H_2L$) Ligand**

| compound | $Fe-N_{im}$ (Å) | $Fe-O_{Ph}$ (Å) | $\Sigma^a$ (°) | ref |
|---|---|---|---|---|
| $NH_4[FeL_2]$ | 2.134[b] | 1.972[c] | 83.9 | 25a |
| $Pr_3N[Fe(3MeO\text{-}L)_2]$ | 2.144[b] | 1.975[c] | 75.0 | 25d |
| $[Fe_2L_2(CH_3OH)_2Cl_2]$ | 2.065(5) | 1.942[b] | 130.8 | 26c |
| [FeL(acac) (dmso)] | 2.133(3) | 1.932[b] | 51.0 | 25c |
| $[\{Fe(3MeO\text{-}L)_2\}_2Tb(NO_3)(H_2O)]$ | 2.160[b] | 1.999[c] | 143.0 | 25d |
| | 2.173[b] | 1.983[c] | 155.0 | |
| **1** | 2.149[b] | 1.987[c] | 80.7 | this work |
| **2** | 2.134[c] | 1.971[c] | 76.9 | this work |
| **3** | | | | |
| cation | 2.104(4) | 1.936[b] | 57.7 | this work |
| anion | 2.148[b] | 1.984[c] | 80.0 | this work |
| **4** | | | | |
| Fe1 | 2.138(3) | 1.984[b] | 64.8 | this work |
| Fe2 | 2.125[b] | 1.997[c] | 101.1 | this work |

[a]The octahedral distortion calculated from 12 *cis* angles found in the coordination polyhedron. [b]The average value calculated from two bond lengths. [c]The average value calculated from four bond lengths. Ligand abbreviations: acac = acetylacetonate, dmso = dimethyl sulfoxide.

*Evaluation of Fe−O···K···O−Fe vs π···π Exchange Magnetic Pathways in $K[FeL_2]\cdot H_2O$ (1).* Polymeric coordination compound $K[FeL_2]\cdot H_2O$ (**1**) can be easily prepared via the reaction of one molar equivalent of $FeCl_3\cdot 6H_2O$ with two equivalents of the $H_2L$ ligand in a methanolic solution, with KOH used as a base for deprotonation. As a result, dark-brown prismatic crystals can be obtained by slow evaporation of the parent solution. The crystal structure consists of the $[FeL_2]^-$ complex anions assembled into a one-dimensional (1D) chain structure by interactions of the $K^+$ cations with phenolate O atoms from the complex anions and water molecules (see Figure 1). The $[FeL_2]^-$ anion has similar bond lengths and angular distortion of the coordination polyhedron corresponding to previously reported compounds containing the $[Fe(R\text{-}L)_2]^-$ anion (Figure 1, Table 2). The lengths of the bridging K···O distances vary between 2.76 Å and 3.05 Å (Figure 1). The water molecule is bonded to the $K^+$ cation over a rather long distance (2.620(2) Å) and it forms a hydrogen bond of moderate strength with the adjacent phenolic O atom: *d*(O 1s···O1) = 2.917(3) Å. Interchain interactions are provided by the face-to-face ring−ring interactions of the neighboring $[FeL_2]^-$ anions, where the entire ligand moiety is involved in the formation of the offset and twisted contact with the centroid-centroid distance of 3.786 Å (Figure 1). The arrangement is further stabilized by the weak C−H···O interactions between the aromatic C−H groups and phenolic O atoms where the closest donor−acceptor distance is observed for the contact involving the C−H donor from the imino group with *d*(C7···O4) = 3.660(3) Å (Figure 1).


DOI: 10.1021/acs.inorgchem.5b01271
*Inorg. Chem.* 2015, 54, 8625−8638

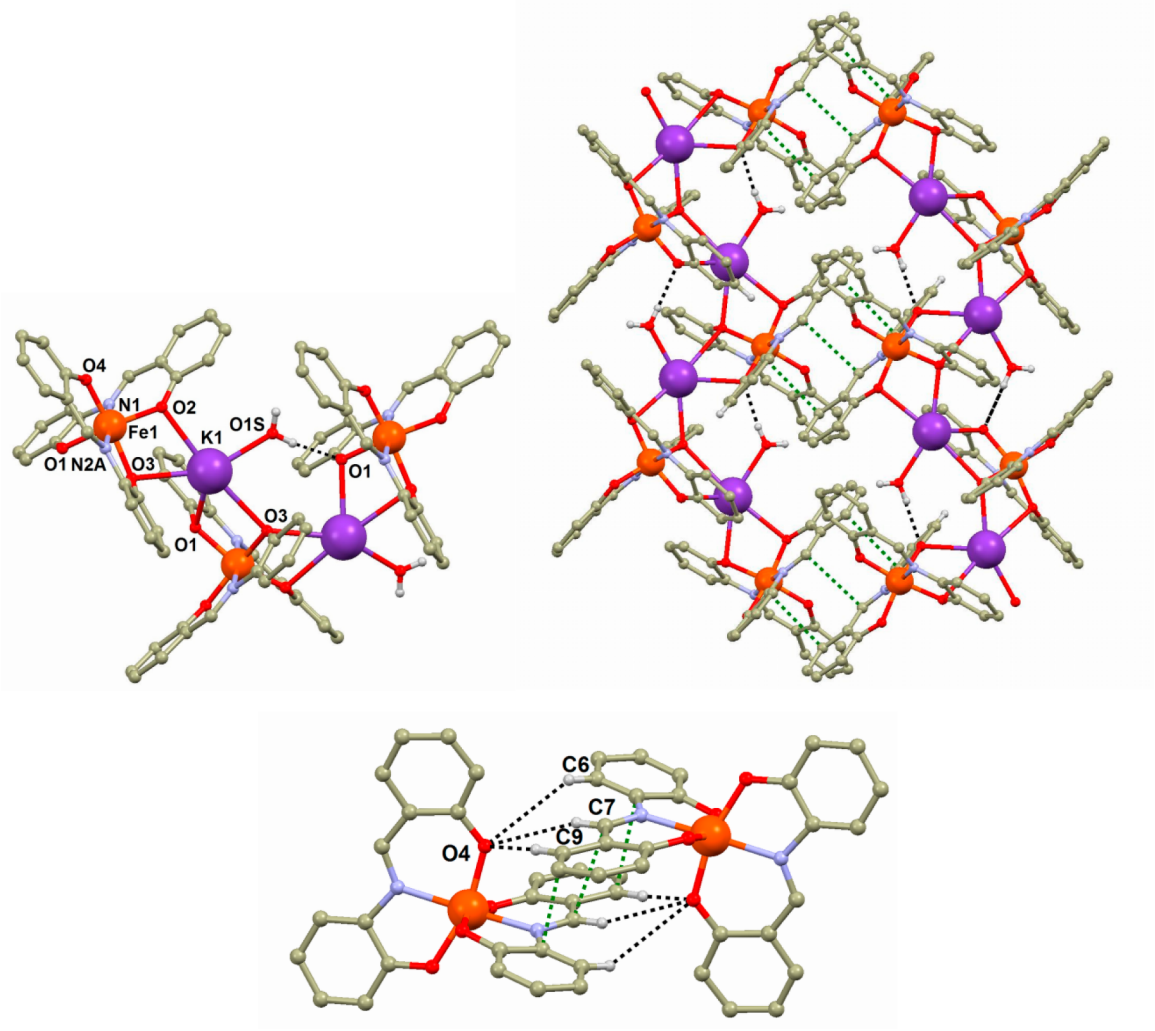


**Figure 1.** (Top left) Perspective view on a fragment of the crystal structure of **1**; hydrogen atoms, except for those involved in noncovalent contacts (black dashed lines), are omitted for the sake of clarity (the donor···acceptor distance is $d$(O1S···O1) = 2.917(3) Å). (Top right) Perspective view of the chain fragments and noncovalent interactions; the short C···C contacts are displayed as green dashed lines. (Bottom) Detailed view on the interchain interactions of the aromatic rings with displayed C−H···O noncovalent contacts. [Selected bond lengths: Fe1−O2 = 1.964(2) Å, Fe1−N1 = 2.137(2) Å, Fe1−O4 = 1.955(2) Å, Fe1−O1 = 2.019(2) Å, Fe1−O3 = 2.007(2) Å, K1···O3 = 3.050(2) Å, K1···O1 = 2.763(2) Å, K1···O1S = 2.620(2) Å, K1···O3 = 2.835(2) Å, K1···O2 = 2.922(2) Å.]

In order to estimate magnetic exchange through the Fe−O···K···O−Fe superexchange pathway, the isotropic exchange was calculated for the $\{[FeL_2]\cdots K(H_2O)\cdots[FeL_2]\}^-$ assembly, using the broken-symmetry state approach at the B3LYP/def2-TZVP level of theory. The spin densities of selected atoms and energetics of HS and BS states are summarized in Table S1 in the Supporting Information. The energy difference ($\Delta$) between the BS state and the HS state was used to calculate the value of $J$, as

$$E_{BS} - E_{HS} = \Delta = J(2S_1S_2 + S_2) = 15J \quad (1)$$

using the following spin Hamiltonian postulated for a dimer:

$$\hat{H} = -J(\vec{S}_1\cdot\vec{S}_2) \quad (2)$$

The resulting value of $J$ is very small: $J = -0.052$ cm$^{-1}$. The spin density is mainly located on the Fe atoms and partially delocalized on the N/O donor atoms of the L ligands (see Figure S1 in the Supporting Information). The spin density on the K atom is negligible—$\rho$(K) = 0.005 for the HS state and $\rho$(K) = −0.0006 for the BS state—which suggests that this coupling path should be very weak. Next, the calculation was performed for a $\pi-\pi$ stacked dimer $\{[K(H_2O)FeL_2]\cdots[FeL_2K(H_2O)]\}$ and resulted in a stronger antiferromagnetic exchange with $J = -0.19$ cm$^{-1}$. The spin densities on the chromophore atoms are very similar and show the spin delocalization on all donor atoms of the L ligands (see Table S1 and Figure S1).

The experimental magnetic data for **1** are displayed in Figure 2. The effective magnetic moment adopts a value of 5.83$\mu_B$, which is close to the theoretical HS state value for $S = 5/2$ (5.92$\mu_B$). The decrease of $\mu_{eff}/\mu_B$ is evident below 25 K and the final value at 1.9 K is 3.38 $\mu_B$. This behavior suggests that non-negligible antiferromagnetic exchange interactions must be present in the solid state. Taking into account the results from the DFT calculations, the following spin Hamiltonian was used:

$$\hat{H} = -J(\vec{S}_1\cdot\vec{S}_2) + \sum_{i=1}^{2} D_i\left(\hat{S}_{i,z}^{\,2} - \hat{S}_i^{\,2}/3\right) + \mu_B B g_i \hat{S}_{i,a} \quad (3)$$

where the isotropic term ($J$) describes the exchange within the $\pi-\pi$ stacked dimer. The zero-field splitting (ZFS) term was added to characterize the magnetic anisotropy, because of



DOI: 10.1021/acs.inorgchem.5b01271
*Inorg. Chem.* 2015, 54, 8625−8638

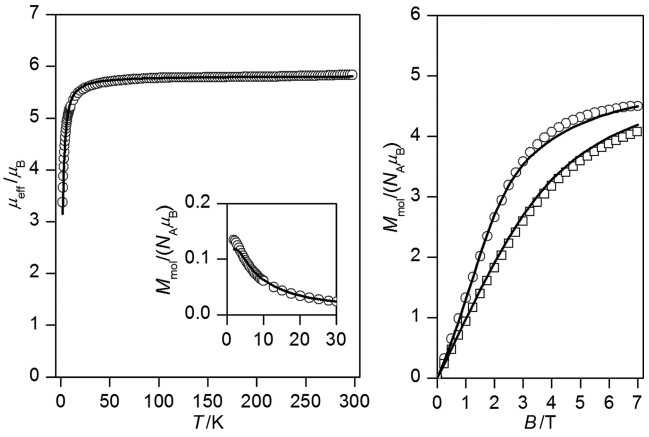


**Figure 2.** Magnetic data for compound **1**. (Left) Temperature dependence of the effective magnetic moment and molar magnetization measured at $B$ = 0.1 T. (Right) Isothermal magnetizations measured at (○) $T$ = 2.0 K (□) and $T$ = 5 K. Symbols represent experimental data; lines represent data calculated using eq 3 and values of $J$ = −0.347(9) cm$^{-1}$, $D$ = +1.6(2) cm$^{-1}$, and $g$ = 1.966(3). Data are scaled per one iron(III) center.

distortion of the pseudo-octahedral heterogeneous chromophore ($a$ = $x$ or $z$). The integral average of the magnetization was calculated to ensure the best simulation of the experimental data measured on a powder sample. Both temperature-dependent and magnetic-field-dependent magnetization data were fitted simultaneously and resulted in $J$ = −0.347(9) cm$^{-1}$, $D$ = +1.6(2) cm$^{-1}$, and $g$ = 1.966(3) (Figure 2).[34] A slightly worse fit was also found for a negative $D$ parameter: $J$ = −0.29(3) cm$^{-1}$, $D$ = −1.2(2) cm$^{-1}$, and $g$ = 1.964(7) (see Figure S2 in the Supporting Information). The fitted $J$-values are close to that derived from the DFT calculations ($J$ = −0.19 cm$^{-1}$). The $|D|$ values are non-negligible and similar values were also found for other iron(III) Schiff-base complexes.[35]

*Evaluation of the π···π Exchange Magnetic Pathway in (Pr$_3$NH)[FeL$_2$]·H$_2$O (2).* Mononuclear complex (Pr$_3$NH)[FeL$_2$]·H$_2$O (**2**) was prepared similarly to previously reported Pr$_3$NH[Fe(3MeO-L)$_2$]·2H$_2$O,[25d] and the preparation procedure is also very similar to that reported here for **1**, except that Pr$_3$N is used as a base instead of KOH. The crystal structure of **2** is composed of the [FeL$_2$]$^-$ complex anions, which are relatively isolated; the only present significant noncovalent interactions are the following: a bifurcated hydrogen bond between the amine N atom from the Pr$_3$NH cation and phenolate O atoms ($d$(N1S···O2/O4) = 2.949(3) and 2.990(4) Å) and offset interactions of the aromatic rings ($d$(centroid···centroid) = 3.6387(1) Å, Figure 3). The [FeL$_2$]$^-$ complex anions have bond lengths and the angular distortion parameter similar to other compounds containing isolated [Fe(R-L)$_2$]$^-$ anions (see Figure 3, Table 2).

According to X-ray analysis, the only relevant intermolecular interactions are between two mononuclear entities mediated by π−π stacking. For that reason, the dinuclear unit {Pr$_3$NH-[FeL$_2$]···[FeL$_2$]Pr$_3$NH} was chosen for DFT calculation of imaginable exchange between the iron(III) centers. The calculation output is summarized in Table S2 in the Supporting Information, and the spin densities are plotted in Figure S3 in the Supporting Information. The BS state is energetically slightly favored, and by utilizing eqs 1 and 2, the calculated isotropic exchange was found to be very weak and antiferromagnetic ($J$ = −0.022 cm$^{-1}$).

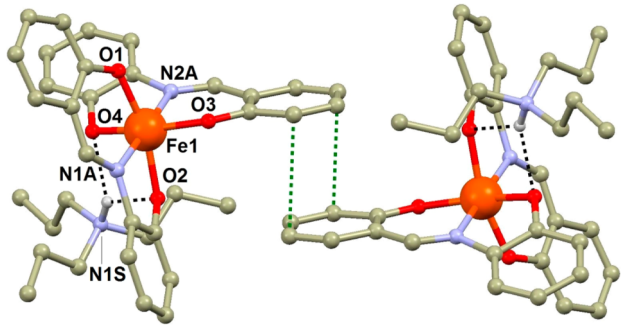


**Figure 3.** Perspective view of the fragment of the crystal structure of **2**. Hydrogen atoms, except for those involved in hydrogen bonding (black dashed lines), are omitted for the sake of clarity. The short C··· C contacts are displayed as green dashed lines. Selected bond lengths: Fe1−N2A = 2.168(4) Å, Fe1−O4 = 2.003(2) Å, Fe1−O2 = 1.985(2) Å, Fe1−N1A = 2.117(4) Å, Fe1−O3= 1.948(2) Å, Fe1−O1 = 1.947(2) Å.

The magnetic data of compound **2** are depicted in Figure 4. In this case, the effective magnetic moment is practically

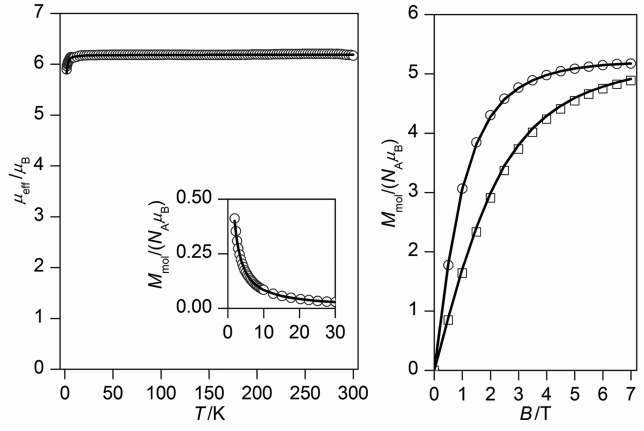


**Figure 4.** Magnetic data for compound **2**. (Left) Temperature dependence of the effective magnetic moment and molar magnetization measured at $B$ = 0.1 T. (Right) Isothermal magnetizations measured at (○) $T$ = 2.0 and (□) $T$ = 4.6 K. Symbols represent experimental data; lines represent the calculated data using eq 3 and $J$ = −0.025(4) cm$^{-1}$, $D$ = −0.48(4) cm$^{-1}$, and $g$ = 2.091(1). Data are scaled per one iron(III) center.

constant ($\mu_{eff}/\mu_B$ = 6.20 at 300 K) down to 5 K and reaches a value of 5.90$\mu_B$ at 2 K. This behavior is in large contrast to the observation for **1** and indicates that intermolecular π−π interactions induce very weak magnetic exchange as a result from DFT calculations. Both temperature- and field-dependent magnetic data sets were treated simultaneously using the spin Hamiltonian for a dimer defined in eq 3. Again, the integral average of the magnetization was used to simulate the powder signal. Very good results were obtained for $J$ = −0.025(4) cm$^{-1}$, $D$ = −0.48(4) cm$^{-1}$, and $g$ = 2.091(1) (Figure 4), but also a solution for a positive $D$ parameter was found ($J$ = −0.038(5) cm$^{-1}$, $D$ = +0.53(8) cm$^{-1}$, and $g$ = 2.091(2); see Figure S4 in the Supporting Information). Both $J$-values are very close to that reported by DFT. The found $|D|$ values are lower than those observed in compound **1**, which can be explained by different effects of K$^+$ and Pr$_3$NH cations on charge distribution of phenolic O atoms directly coordinated to central atom.



DOI: 10.1021/acs.inorgchem.5b01271
*Inorg. Chem.* 2015, 54, 8625−8638

**Supramolecular Dimer: The Exchange Interaction Going through a Strong Hydrogen Bond.** Compound $[FeL(bpyO_2)(CH_3OH)][FeL_2]\cdot CH_3OH$ (**3**) can be easily prepared by mixing of methanolic solutions of **2** and $[FeL(bpyO_2)(H_2O)]Cl$ (**3′**) and it crystallizes as black prismatic crystals. It consists of the complex cation $[FeL(bpyO_2)(CH_3OH)]^+$, which binds the $[FeL_2]^-$ complex anion by a relatively strong hydrogen bond between the coordinated molecule of methanol and phenolic O atom (Figure 5): $d$(O9···O2) = 2.580(3) Å. Again, the $[FeL_2]^-$ complex anions have bond lengths and angular distortion parameters similar to other compounds containing isolated $[Fe(R\text{-}L)_2]^-$ anions (Figure 5, Table 2).

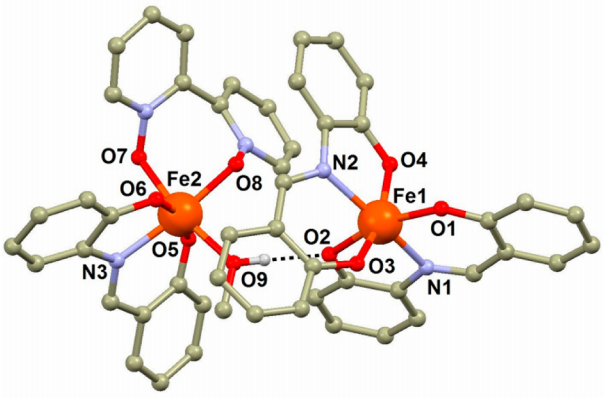


**Figure 5.** Perspective view of the fragment of the crystal structure of **3**. Hydrogen atoms, except for those involved in hydrogen bonding (black dashed lines), are omitted for the sake of clarity. Selected bond lengths: Fe1–O3 = 1.958(2) Å, Fe1–N2 = 2.145(3) Å, Fe1–O1 = 1.943(3) Å, Fe1–O4 = 2.006(1) Å, Fe1–N1 = 2.151(3) Å, Fe1–O3 = 1.958(2) Å, Fe1–O2 = 2.030(2) Å, Fe2–O7 = 2.034(2) Å, Fe2–O8 = 1.999(2) Å, Fe2–O6 = 1.938(2) Å, Fe2–N3A = 2.103(4) Å, Fe2–O5 = 1.933(2) Å, Fe2–O9 = 2.054(2) Å.

On the other hand, the $[FeL(bpyO_2)(CH_3OH)]^+$ cations have much smaller angular distortions than complex anions ($\Sigma$ = 57.7° vs 80.0°, Table 2). This is mainly due to the lower rigidity of their coordination polyhedron coming from the heteroleptic coordination environment with the flexible $bpyO_2$ ligand and monodentate methanol molecule.

The metal–ligand bond lengths between the Fe atom and O atoms from the $bpyO_2$ ligand ($O_{bpy}$) or $CH_3OH$ ($O_M$) are slightly longer than those typically observed for Fe–$O_{Ph}$ bonds for compounds containing the $L^{2-}$ ligand: $d$(Fe–$O_{bpy}$) = 2.034(2) and 1.999(2) Å, $d$(Fe–$O_M$) = 2.054(2) Å (Figure 5, Table 2).

The dominant superexchange pathway is expected through the H-bond mediated by the O–H group of methanol between the complex cation and complex anion –{$[FeL(bpyO_2)(CH_3OH)]$···$[FeL_2]$.$CH_3OH$}. The DFT calculations for this moiety are summarized in Table S3 and Figure S5 in the Supporting Information. The BS state is also lower in energy in this case, resulting in the antiferromagnetic exchange with the value of $J$ = −0.53 $cm^{-1}$.

The magnetic behavior of **3** is plotted in Figure 6 and it is in agreement with the DFT results, i.e., weak antiferromagnetic exchange is confirmed by declination of the effective magnetic moment below 25 K. The theoretical analysis was performed with the spin Hamiltonian for a dimer (eq 3); however, in this case, there are two nonequivalent Fe(III) atoms, so the relation

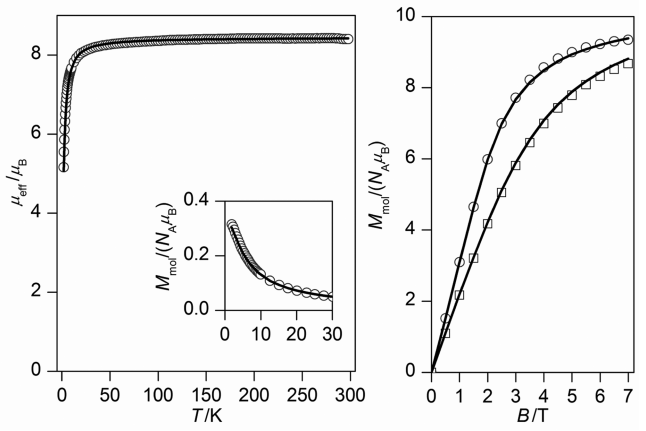


**Figure 6.** Magnetic data for compound **3**. (Left) Temperature dependence of the effective magnetic moment and molar magnetization measured at $B$ = 0.1 T. (Right) Isothermal magnetizations measured at (○) $T$ = 2.0 and (□) $T$ = 4.6 K. Symbols represent experimental data; lines represent calculated data using eq 3 and $J$ = −0.41(1) $cm^{-1}$, $D_1$ = +2.2(4) $cm^{-1}$, $D_2$ = −0.06(7) $cm^{-1}$, and $g$ = 2.018(2).

$D_1 \neq D_2$ holds. We tried several combinations of the starting values for $D_1$ and $D_2$ parameters in fitting procedure and satisfactory results were obtained for $J$ = −0.41(1) $cm^{-1}$, $D_1$ = +2.2(4) $cm^{-1}$, $D_2$ = −0.06(7) $cm^{-1}$, and $g$ = 2.018(2) (see Figure 6). The large difference between $D_1$ and $D_2$ values reflects different nature of the ligands in the complex cation and complex anion of **3**, hence their different chromophores $\{FeNO_5\}$ and $\{FeN_2O_4\}$, as well as different octahedral distortion parameters ($\Sigma$ = 57.7° and $\Sigma$ = 80.0°, respectively). We can further speculate that larger $\Sigma$-parameter would manifest itself in larger magnetic anisotropy; however, such simple magneto-structural correlation was not confirmed in our previous studies, even for iron(III) complexes with the same type of the chromophores;[3Sa,d] therefore, the larger single-ion $D$ parameter cannot be unambiguously assigned to the Fe1 atom in the complex anion of compound **3**.

**Covalently Bonded Polynuclear Fe(III) Complexes.** $[Fe_2L_3(CH_3OH)]\cdot 2CH_3OH\cdot H_2O$ (**4**) was prepared by the reaction of **2** with the previously reported $[Fe_2L_2(CH_3OH)_2Cl_2]$ in the molar ratio of 2:1. Crystallographic analysis revealed a dinuclear molecular structure, which consists of two parts: the $[FeL(CH_3OH)]^+$ moiety is "coordinated" through the phenolate O atoms belonging to the $[FeL_2]^-$ subunit (Figure 7). When inspecting bond lengths and angular distortion parameters in $[FeL_2]^-$, the following basic difference in comparison with other compounds containing isolated $[Fe(R\text{-}L)_2]^-$ anions can be found: the Fe–$O_{Ph}$ bond lengths are slightly longer and angular distortion is significantly larger. Both observed enlargements are due to the bridging function of two $O_{Ph}$ atoms: the nonbridging Fe–$O_{Ph}$ bonds are shorter (1.894(2), 1.977(2) Å) than the bridging ones (2.014(2), 2.101(2) Å). Covalent superexchange pathway is provided by two Fe1–$O_{Ph}$–Fe2 linkages (Figure 7) with the Fe1···Fe2 distance of 3.2130(5) Å. A possible noncovalent exchange pathway can be found between dinuclear moieties provided by noncovalent interactions of aromatic rings (the shortest C···C distance is 3.363(5) Å) and by relatively short C–H···O contacts ($d$(C33···O4) = 3.248(3) Å, $d$(C31···O4) = 3.394(3) Å, Figure 7). Lattice solvents (two methanol and one water molecules) together with coordinated methanol molecule


DOI: 10.1021/acs.inorgchem.5b01271
Inorg. Chem. 2015, 54, 8625–8638

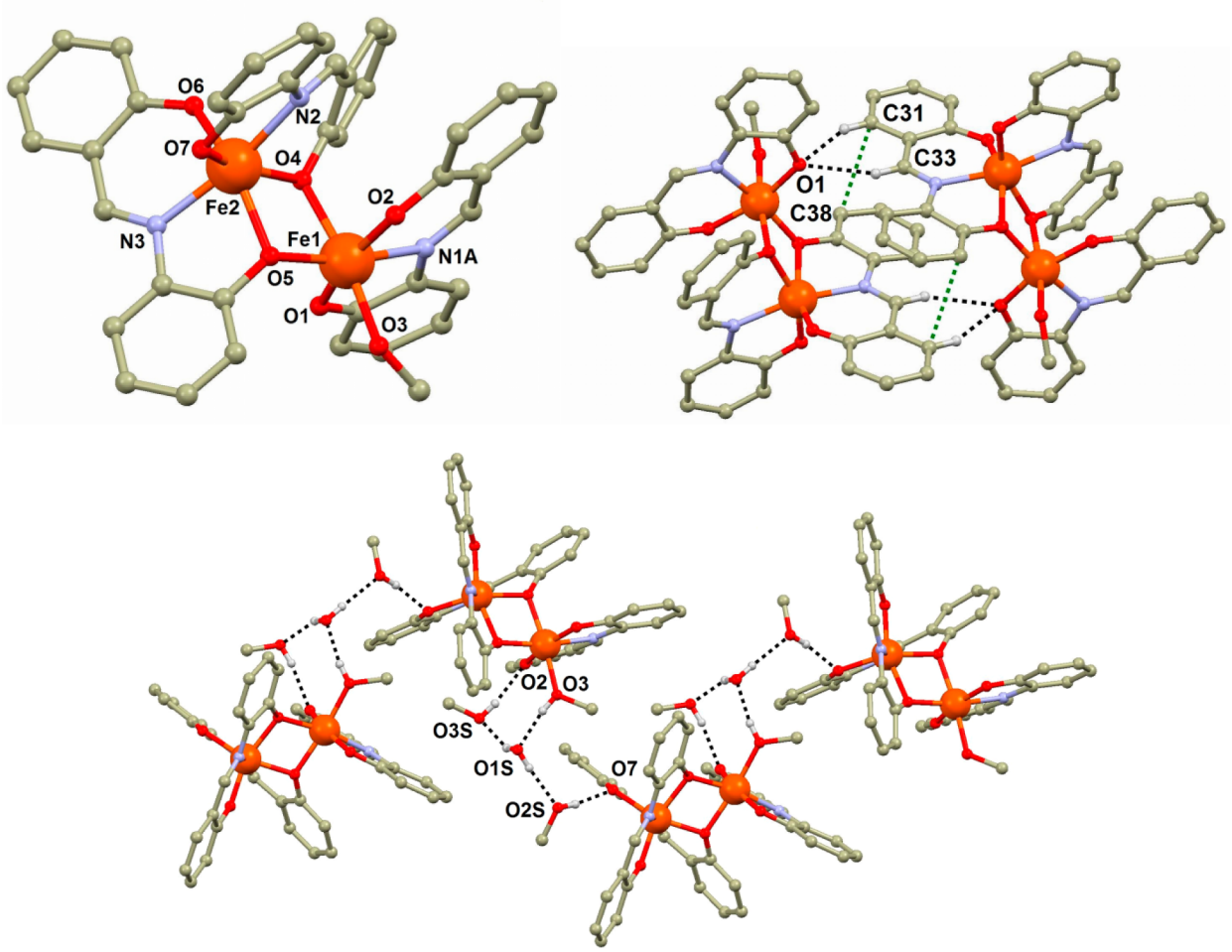


**Figure 7.** (Top left) Molecular structure of compound **4**. Selected bond lengths: Fe2−N3= 2.100(2) Å, Fe2−O5 = 2.101(2) Å, Fe2−O4= 2.014(2) Å, Fe2−N2 = 2.149(2) Å, Fe2−O6 = 1.894(2) Å, Fe2−O7= 1.977(2) Å, Fe1−O5 = 2.006(2) Å, Fe1−O4 = 2.054(2) Å, Fe1−O2 = 1.945(2) Å, Fe1−N1A = 2.138(3) Å, Fe1−O1 = 1.931(2) Å, Fe1−O3 = 2.074(2) Å. (Top right) Perspective view of the interconnection of two dinuclear $[Fe_2L_3(CH_3OH)]$ molecules by C−H···O noncovalent interactions. Short C···C contacts are displayed as green dashed lines. (Bottom) Perspective view of the hydrogen bonding in the crystal structure of **4**. Hydrogen atoms, except for those involved in hydrogen bonding (black dashed lines), are omitted for the sake of clarity. The donor···acceptor distances: $d$(O1S···O3S) = 2.692(4) Å, $d$(O1S···O2S) = 2.700(4) Å, $d$(O2S···O7) = 2.740(3) Å, $d$(O3···O1S) = 2.576(3) Å, $d$(O3S···O2) = 2.746(3) Å.

**Table 3. B3LYP/def2-TZVP Calculated Net Mulliken Spin Densities, the $\langle S^2 \rangle$ Values and Relative Energies of BS States for the Supramolecular Tetranuclear Moiety $\{[Fe_2L_3(CH_3OH)]\}_2$ of 4**

| spin state | $\langle S^2 \rangle$ | $\Delta_i$ (cm$^{-1}$)[a] | $\rho$(Fe1) | $\rho$(Fe2) | $\rho$(Fe2′) | $\rho$(Fe4) |
|---|---|---|---|---|---|---|
| HS, $\lvert\alpha\alpha\alpha\alpha\rangle$ | 110.04 | 0 | 4.23 | 4.20 | 4.23 | 4.20 |
| BS1, $\lvert\beta\alpha\alpha\alpha\rangle$ | 35.01 | −227.2835 | −4.22 | 4.19 | 4.23 | 4.20 |
| BS2, $\lvert\alpha\beta\alpha\alpha\rangle$ | 35.01 | −227.1058 | 4.22 | −4.19 | 4.23 | 4.20 |
| BS12, $\lvert\beta\beta\alpha\alpha\rangle$ | 10.04 | −7.5763 | −4.23 | −4.20 | 4.23 | 4.20 |

[a] $\Delta_i = \varepsilon_{BS,i} - \varepsilon_{HS}$.

form supramolecular chains via O−H···O hydrogen bonding (Figure 7, bottom).

This dinuclear compound (**4**) is the first complex of the reported series in which the dominant magnetic interaction between the iron centers is mediated through covalent bonds. First, the DFT calculations were performed for this dinuclear unit $\{[Fe_2L_3(CH_3OH)]\}$ of **4**, and the results are reported in Table S4 and Figure S6 in the Supporting Information. The BS state is lower in energy again, and we found the isotropic exchange value of $J = -13.8$ cm$^{-1}$ by using eqs 1 and 2, thus suggesting antiferromagnetic interaction of intermediate strength in **4**. Second, the DFT calculations were done for a supramolecular tetranuclear unit (Figure 7) with the aim to identify other weaker magnetic interactions. Hence, the following spin Hamiltonian was postulated:

$$\hat{H} = -J_{12}(\vec{S}_1 \cdot \vec{S}_2 + \vec{S}_{1'} \cdot \vec{S}_{2'}) - J_{12'}(\vec{S}_1 \cdot \vec{S}_{2'} + \vec{S}_{1'} \cdot \vec{S}_2) - J_{22'}(\vec{S}_2 \cdot \vec{S}_{2'}) \quad (4)$$

where $J_{12}$ is the isotropic exchange within the covalently bridged dimers (Fe1−Fe2 and Fe1′−Fe2′), $J_{12'}$ is the isotropic exchange between the Fe1−Fe2′ and Fe1′−Fe2 centers involving the Fe−O···H−C → Fe noncovalent interaction and $J_{22'}$ is the isotropic exchange between Fe2−Fe2′ mediated through $\pi$−$\pi$ stacking.



DOI: 10.1021/acs.inorgchem.5b01271
Inorg. Chem. 2015, 54, 8625−8638

To determine these three $J$ values, the BS states were calculated by flipping spins on Fe1 and Fe2, and simultaneously on both Fe1 and Fe2 atoms, resulting in energy differences $\Delta_1$, $\Delta_2$, and $\Delta_{12}$, respectively (see Table 3 and Figure S7 in the Supporting Information). The solution of linear equations derived for different spin states then led to these formulas for the isotropic exchange constants:

$$J_{12} = \frac{\Delta_1 + \Delta_2 - \Delta_{12}}{30}$$

$$J_{12'} = \frac{\Delta_1 - \Delta_2 + \Delta_{12}}{30}$$

$$J_{22'} = \frac{\Delta_2 - \Delta_1}{15} \quad (5)$$

Utilizing the calculated energy differences $\Delta_i$, the numerical values were found to be $J_{12} = -14.9$ cm$^{-1}$, $J_{12'} = -0.26$ cm$^{-1}$ and $J_{22'} = +0.012$ cm$^{-1}$. Remarkably, these data suggest that the C−H···O noncovalent interaction is a more efficient superexchange pathway than $\pi-\pi$ stacking.

The experimental magnetic properties agree well with the DFT theoretical prediction (Figure 8). The effective magnetic moment has a room-temperature value of 7.87$\mu_B$, which is lower than the theoretical value of 8.37$\mu_B$ for two noninteracting $^5/_2$–$^5/_2$ spins, and it rapidly decreases upon cooling to 1.05$\mu_B$ at $T$ = 1.9 K. The molar susceptibility experiences the maximum at $T$ = 45 K, which is a fingerprint for antiferromagnetically coupled homospin dimers. The nonzero low-temperature value of $\mu_{eff}$ due to the increase of susceptibility below 4 K suggests the presence of a small amount of monomeric impurities. The magnetic data were treated with eq 3, but only isotropic terms were included, because the large separation of the singlet ground state from the excited state with $S > 0$ prevents us from uncovering information about magnetic anisotropy. The total magnetization of the powder sample was calculated as the sum of the contributions of a dimer and monomeric paramagnetic impurity, $M_{mol} = (1 - x_{PI})M_{dimer} + 2x_{PI}M_{mono}$. The best result was obtained for $J = -12.3(9)$ cm$^{-1}$, $g = 2.061(4)$, and $x_{PI} = 1.31(4)$% (Figure 8). The all three parameters sets were used to calculate the magnetic properties, and these data are plotted in Figure 8, showing good concordance.

Tetranuclear complex $[\{Fe_2L_2\}(\mu\text{-}OH)_2\{FeL(bpyO_2)\}_2][BPh_4]_2\cdot 2H_2O$ (**5**) was prepared by the reaction of $[Fe_2L_2(CH_3OH)_2Cl_2]$ with $[FeL(bpyO_2)(H_2O)]Cl$ in the molar ratio of 1:1 in the presence of bulky $BPh_4^-$ anions. The crystal structure of **5** consists of the $[\{Fe_2L_2\}(\mu\text{-}OH)_2\{FeL(bpyO_2)\}_2]^{2+}$ cations, two $BPh_4^-$ anions and crystal lattice water molecules. The structure of the $[\{Fe_2L_2\}(\mu\text{-}OH)_2\{FeL(bpyO_2)\}_2]^{2+}$ cation is depicted in Figure 9, and it consists of the central $[Fe_2L_2]^{2+}$ moiety, which is connected with two peripheral $[FeL(bpyO_2)]^+$ cations. Bridging between the above-mentioned moieties is provided by the $O_{Ph}$ atoms from the aminophenolic parts of the $[FeL(bpyO_2)]^+$ cation subunits and by hydroxy bridging ligands (Figure 9). The central $[Fe_2L_2]^{2+}$ moiety is significantly twisted in comparison with the same fragment in the structure of $[Fe_2L_2(CH_3OH)_2Cl_2]$; however, bridging within this dimeric unit is provided in very similar fashion by the $O_{Ph}$ atoms from the aminophenolic parts of the ligands. The intramolecular Fe···Fe distances are very similar, ranging between 3.13 Å and 3.20 Å (Figure 9).

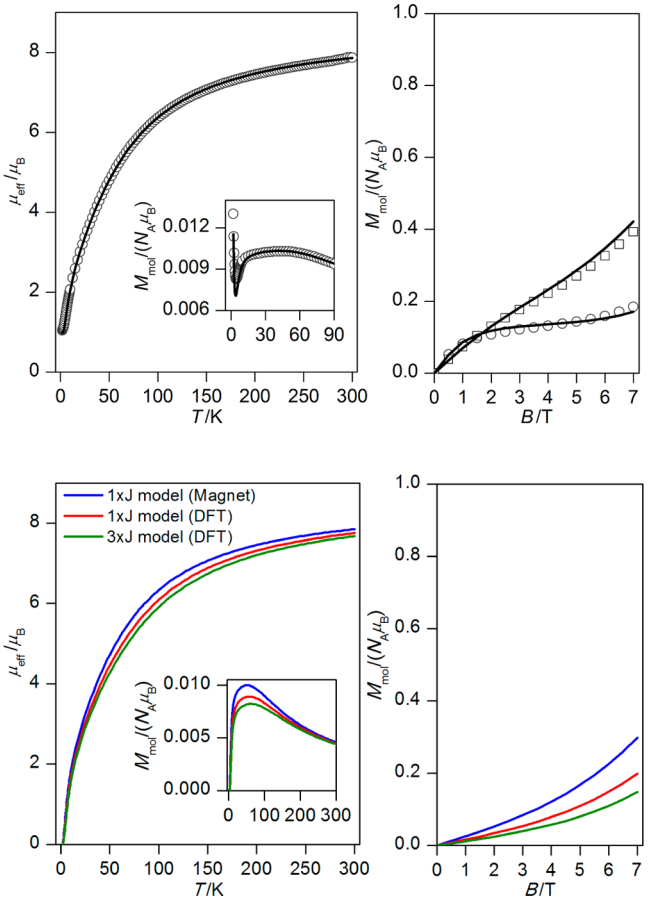


**Figure 8.** (Top) Magnetic data for compound **4**: the temperature dependence of the effective magnetic moment is shown, with the inset showing the molar magnetization measured at $B$ = 0.1 T, and the isothermal magnetizations measured at (○) $T$ = 2.0 and (□) $T$ = 4.6 K. Symbols represent experimental data; lines represent calculated data using eq 3 and $J = -12.3(9)$ cm$^{-1}$, $g = 2.061(4)$, and $x_{PI} = 1.31(4)$%. (Bottom) Comparison of magnetic properties for **4**, calculated using either the 2-$J$ model defined in eq 3, using fitted parameters from experimental magnetic data ($J = -12.3$ cm$^{-1}$, $g = 2.06$, blue color), and using the calculated parameter from DFT on dimeric moiety ($J = -13.8$ cm$^{-1}$, red color) or the 3-$J$ model defined in eq 4, using parameters calculated by DFT on tetrameric moiety ($J_{12} = -14.9$ cm$^{-1}$, $J_{12'} = -0.26$ cm$^{-1}$, and $J_{22'} = +0.012$ cm$^{-1}$, green color). The isothermal magnetization data were calculated for $T$ = 4.6 K. All data are scaled per two iron(III) centers.

From the information acquired by analyzing the molecular structure of **5**, we may conclude that the most dominant magnetic interaction should be among the neighboring Fe atoms either through the ($\mu$-$O_{Ph}$, $\mu$-OH) fashion (Fe1−Fe2 and Fe3−Fe4) or through bis($\mu$-$O_{Ph}$) bridge (Fe2−Fe3). Moreover, we must also take into account possible exchange through intramolecular hydrogen bond between the terminal Fe atoms (Fe1−OH···O−Fe4, $d$(Fe1−Fe4) = 5.326 Å). However, the interatomic distances between the Fe1−Fe3 and Fe2−Fe4 atoms are even smaller (4.562 and 4.951 Å) which gives the possibility for next-neighbor interactions. To dissect all these possibilities, the following spin Hamiltonian was postulated:

$$\hat{H} = -J_{12}(\vec{S}_1\cdot\vec{S}_2) - J_{23}(\vec{S}_2\cdot\vec{S}_3) - J_{34}(\vec{S}_3\cdot\vec{S}_4) - J_{14}(\vec{S}_1\cdot\vec{S}_4) - J_{13}(\vec{S}_1\cdot\vec{S}_3) - J_{24}(\vec{S}_2\cdot\vec{S}_4) \quad (6)$$



DOI: 10.1021/acs.inorgchem.5b01271
Inorg. Chem. 2015, 54, 8625−8638

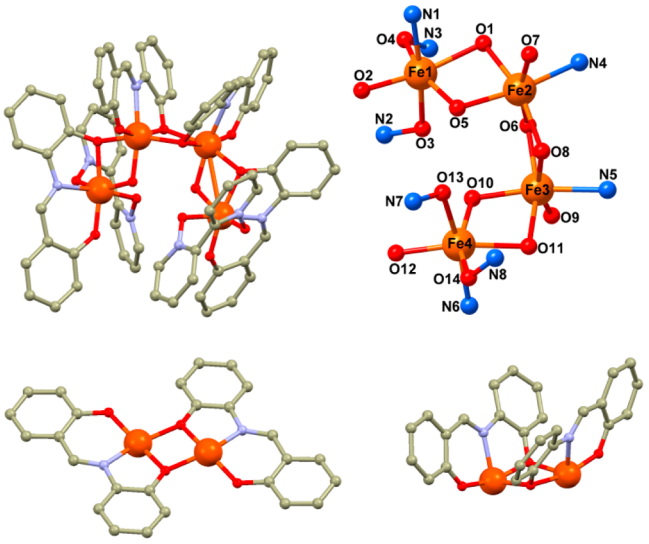


**Figure 9.** (Top left) Molecular structure of $[\{Fe_2L_2\}(\mu\text{-}OH)_2\{FeL(bpyO_2)\}_2]^{2+}$ cation. (Top right) Detailed view of the Fe4 core with the atom labeling scheme. Selected bond lengths: Fe1−O3 = 2.072(2) Å, Fe1−O4 = 2.033(1) Å, Fe1−O2 = 1.904(2) Å, Fe1−N1 = 2.091(2) Å, Fe1−O1 = 2.082(2) Å, Fe1−O5 = 1.940(1) Å, Fe2−O1 = 2.067(1) Å, Fe2−O5 = 1.957(2) Å, Fe2−O6 = 1.882(2) Å, Fe2−O7 = 2.088(2) Å, Fe2−N4 = 2.106(2) Å, Fe2−O8 = 2.046(1) Å, Fe3−O8 = 2.084(2) Å, Fe3−O7 = 2.021(1) Å, Fe3−N5 = 2.128(2) Å, Fe3−O9 = 1.886(2) Å, Fe3−O10 = 1.962(2) Å, Fe3−O11 = 2.064(1) Å, Fe4−O11 = 2.092(2) Å, Fe4−O10 = 1.930(1) Å, Fe4−O13 = 2.063(2) Å, Fe4−N6 = 2.119(2) Å, Fe4−O12 = 1.907(2) Å, Fe4−O14 = 2.040(1) Å, Fe1−Fe2 = 3.1284(4) Å, Fe2−Fe3 = 3.1978(5) Å, Fe3−Fe4 = 3.1551(5) Å. Comparison of the structures of the $[Fe_2L_2]^{2+}$ fragments in $[Fe_2L_2(CH_3OH)_2Cl_2]$ (bottom left) and in **5** (bottom right).

To be able to analyze all six potential magnetic exchange interactions $J_{ij}$, the several BS states are calculated as outlined in Table 4. Using the following Ruiz's approach for calculation of

**Table 4. B3LYP/def2-TZVP Calculated Net Mulliken Spin Densities, the $\langle S^2\rangle$ Values, and Relative Energies of BS States for 5, Based on the Experimental (X-ray) Geometry**

| spin state | $\langle S^2\rangle$ | $\Delta_i$ (cm$^{-1}$)[a] | $\rho$(Fe1) | $\rho$(Fe2) | $\rho$(Fe3) | $\rho$(Fe4) |
|---|---|---|---|---|---|---|
| HS, $\lvert\alpha\alpha\alpha\alpha\rangle$ | 110.04 | 0 | 4.22 | 4.25 | 4.25 | 4.22 |
| BS1, $\lvert\beta\alpha\alpha\alpha\rangle$ | 35.01 | −255.554 | −4.20 | 4.23 | 4.25 | 4.21 |
| BS2, $\lvert\alpha\beta\alpha\alpha\rangle$ | 34.99 | −343.210 | 4.20 | −4.22 | 4.24 | 4.21 |
| BS3, $\lvert\alpha\alpha\beta\alpha\rangle$ | 34.99 | −386.945 | 4.22 | 4.24 | −4.22 | 4.20 |
| BS14, $\lvert\beta\alpha\alpha\beta\rangle$ | 9.97 | −543.250 | −4.20 | 4.23 | 4.23 | −4.20 |
| BS12, $\lvert\beta\beta\alpha\alpha\rangle$ | 10.02 | −103.827 | −4.22 | −4.24 | 4.24 | 4.21 |
| BS13, $\lvert\beta\alpha\beta\alpha\rangle$ | 9.95 | −639.916 | −4.20 | 4.22 | −4.22 | 4.20 |

[a] $\Delta_i = \varepsilon_{BS,i} - \varepsilon_{HS}$.

$J$-parameters, we derived these expressions for the individual $J$ values:

$$J_{12} = \frac{\Delta_1 + \Delta_2 - \Delta_{12}}{30}$$

$$J_{23} = \frac{\Delta_2 + \Delta_3 - \Delta_{14}}{30}$$

$$J_{34} = \frac{-\Delta_1 - \Delta_2 + \Delta_{13} + \Delta_{14}}{30}$$

$$J_{14} = \frac{-\Delta_2 - \Delta_3 + \Delta_{12} + \Delta_{13}}{30}$$

$$J_{13} = \frac{\Delta_1 + \Delta_3 - \Delta_{13}}{30}$$

$$J_{24} = \frac{-\Delta_1 - \Delta_3 + \Delta_{12} + \Delta_{14}}{30} \quad (7)$$

Figure 10 shows the calculated spin density distribution using B3LYP for the $[\{Fe_2L_2\}(\mu\text{-}OH)_2\{FeL(bpyO_2)\}_2]^{2+}$ unit of **5** for the HS and selected BS states (BS13). By using the energy differences $\Delta_i$ between the BS and HS states listed in Table 4, the following isotropic exchange constants were found: $J_{12} = -16.50$ cm$^{-1}$, $J_{23} = -6.23$ cm$^{-1}$, $J_{34} = -19.48$ cm$^{-1}$, $J_{14} = -0.45$ cm$^{-1}$, $J_{13} = -0.086$ cm$^{-1}$, and $J_{24} = -0.15$ cm$^{-1}$. This implies that the effective path for AF-exchange is through the hetero ($\mu$-$O_{Ph}$, $\mu$-OH) bridge, while the homo bis($\mu$-$O_{Ph}$) bridge is almost one-third less effective. The other interactions are all very weak and antiferromagnetic in nature, and the interaction mediated by hydrogen bonds between the terminal centers ($J_{14}$) is the most important one of them.

The experimental magnetic properties of compound **5** are depicted in Figure 11. The effective magnetic moment at room temperature has a value of 10.36$\mu_B$, which is slightly lower than the theoretical value of 11.83$\mu_B$ for four noninteracting $S_i = {}^5/_2$ spins, and it quickly decreases upon cooling to 1.07$\mu_B$ at $T$ = 2.0 K. The maximum of molar susceptibility is found at $T$ = 70 K, which confirms strong antiferromagnetic interactions. The nonzero low-temperature value of $\mu_{eff}$, which is due to the increase in susceptibility at $T$ < 3 K, suggests the presence of a small amount of monomeric impurities. First, the magnetic data were treated with a simplified version of eq 6, in which only dominant contributions were encountered:

$$\hat{H} = -J_1(\vec{S}_1\cdot\vec{S}_2 + \vec{S}_3\cdot\vec{S}_4) - J_2(\vec{S}_2\cdot\vec{S}_3) + \mu_B Bg\sum_{i=1}^{4}\hat{S}_{i,z} \quad (8)$$

The ZFS terms were excluded, because the excited spin states with $S$ > 0, which bear information about magnetic anisotropy, are well separated from the ground state; hence, the low-temperature data are not very informative. The total magnetization of the powder sample was calculated as the sum of the contributions of a tetramer and monomeric paramagnetic impurity:

$$M_{mol} = (1 - x_{PI})M_{tetramer} + 4x_{PI}M_{mono}$$

The best results were obtained for $J_1 = -17.1(2)$ cm$^{-1}$, $J_2 = -5.6(6)$ cm$^{-1}$, $g$ = 2.02(1), and $x_{PI}$ = 0.78(4)% (see Figure 11). These values are in very good agreement with the DFT-derived averaged values $J_1^{DFT} = (J_{12} + J_{34})/2 = -18.0$ cm$^{-1}$, and $J_2^{DFT} = J_{23} = -6.23$ cm$^{-1}$, respectively. As the fit describes the experimental data very well, more-complicated spin Hamiltonians with more interactions would lead to overparametrization and ambiguity of fitted parameters.



DOI: 10.1021/acs.inorgchem.5b01271
Inorg. Chem. 2015, 54, 8625−8638

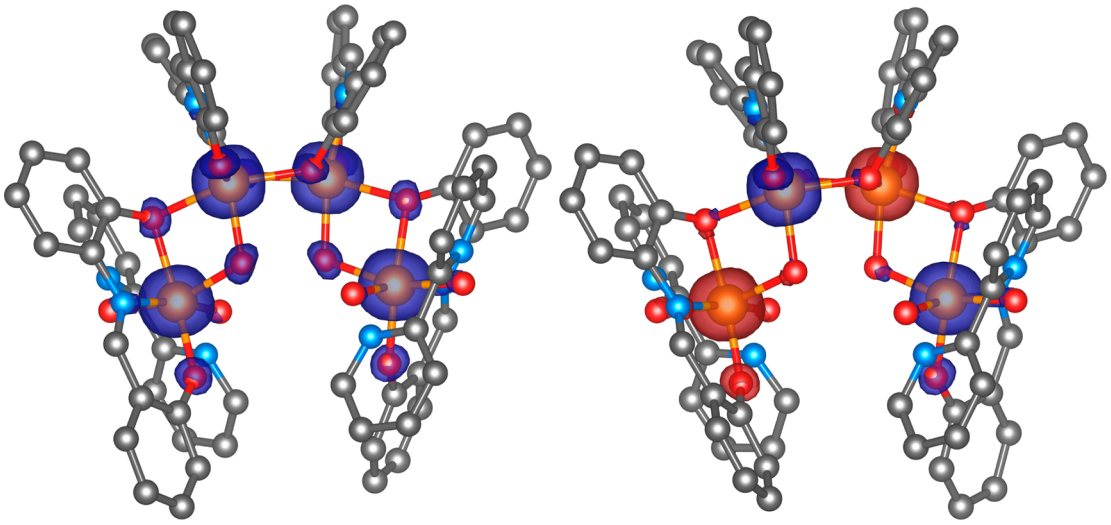

**Figure 10.** Calculated spin density distribution using B3LYP for the $[\{Fe_2L_2\}(\mu\text{-}OH)_2\{FeL(bpyO_2)\}_2]^{2+}$ unit of **5** for the HS and selected BS states (BS13). Positive and negative spin densities are represented by dark blue and dark red surfaces, respectively. The isodensity surfaces are plotted with the cutoff values of $0.02ea_0^{-3}$.

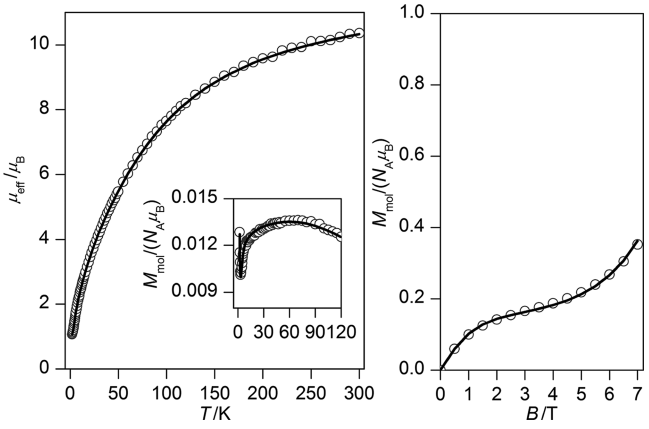


**Figure 11.** Magnetic data for compound **5**. (Left) Temperature dependence of the effective magnetic moment and molar magnetization measured at $B$ = 0.1 T. (Right) Isothermal magnetizations measured at $T$ = 2.0 K. Circles represent experimental data; lines represent calculated data using eq 8 and $J_1 = -17.1(2)$ cm$^{-1}$, $J_2 = -5.6(6)$ cm$^{-1}$, $g = 2.02(1)$, and $x_{PI} = 0.78(4)\%$.

Nevertheless, we compared the calculated magnetic properties for **5** using the 2-$J$ model with the parameters derived from the experimental data and the 6-$J$ model with the parameter calculated by the DFT approach, and they are almost identical (Figure 12), which confirms very good applicability of the B3LYP/def2-TZVP method and its usefulness in assessing the magnetic exchange interactions in polynuclear species.

## DISCUSSION

First, we would like to discuss noncovalent contacts leading to magnetic exchanges. By comparing results of the isotropic exchange parameters for compounds **1**, **2**, and **4**, in which either only $\pi-\pi$ stacking or both $\pi-\pi$ stacking and C−H···O noncovalent contacts are present, we can conclude that stronger antiferromagnetic exchange was observed/calculated in systems were C−H···O noncovalent contacts were also involved. This would suggest that the role of $\pi-\pi$ stacking in propagating magnetic exchange is minor, which is in agreement with, e.g., theoretical work published by Bandeira et al. for

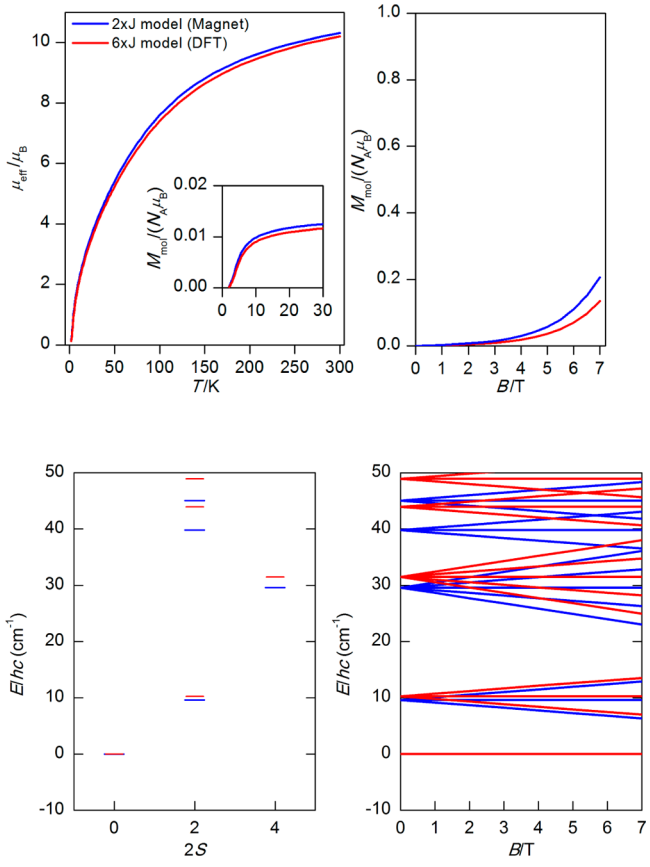


**Figure 12.** Comparison of magnetic properties (top) and energy levels (bottom) for **5** calculated either by the 2-$J$ model defined in eq 8, using the fitted parameters from the experimental magnetic data ($J_1 = -17.1(2)$ cm$^{-1}$, $J_2 = -5.6(6)$ cm$^{-1}$, $g = 2.02(1)$), or by the 6-$J$ model defined in eq 6, using the parameters calculated by DFT ($J_{12} = -16.50$ cm$^{-1}$, $J_{23} = -6.23$ cm$^{-1}$, $J_{34} = -19.48$ cm$^{-1}$, $J_{14} = -0.45$ cm$^{-1}$, $J_{13} = -0.086$ cm$^{-1}$ and $J_{24} = -0.15$ cm$^{-1}$); the isothermal magnetization was calculated for $T$ = 2 K.

copper(II) complexes.[36] However, there are other examples in the literature showing that $\pi-\pi$ stacking can result in significant



DOI: 10.1021/acs.inorgchem.5b01271
Inorg. Chem. 2015, 54, 8625−8638

**Table 5. Comparison of Selected Structural Parameters of Compounds 4-5 and *J* Values Derived from Magnetic Analysis, DFT Calculations and Magnetostructural Correlations from the Literature Data**

| compound | $P$(Fe−O)[a] ($10^{-10}$ m) | $\alpha$(Fe−O−Fe)[b] (deg) | $J^{Lipp}$ ($cm^{-1}$) | $J^{exp}$ ($cm^{-1}$) | $J^{P}$ ($cm^{-1}$) | $J^{\alpha}$ ($cm^{-1}$) | $J^{DFT}$ ($cm^{-1}$) | $J^{mag}$ ($cm^{-1}$) |
|---|---|---|---|---|---|---|---|---|
| **4** (Fe1−Fe2) | 2.0340 | 103.64 | −5.7 | −9.0 | +22.7 | −16.5 | −13.8<br>−14.9 | −12.3(9) |
| **5** (Fe1−Fe2) | 1.9485 | 102.33 | −16.9 | −22.5 | −32.0 | −11.3 | −15.2 | −17.1(2) |
| **5** (Fe2−Fe3) | 2.0545 | 101.84 | −4.4 | −7.3 | +23.2 | −9.3 | −6.4 | −5.6(6) |
| **5** (Fe3−Fe4) | 1.9460 | 103.56 | −17.4 | −23.1 | −33.3 | −16.1 | −17.7 | −17.1(2) |

[a]*P* is a parameter that is defined as half the shortest superexchange pathway between two iron(III) ions. [b]$\alpha$ is defined as the average Fe−O−Fe angle.

exchange parameters, see, e.g., the work by Rajnák et al.,[37] where the authors observed a relatively strong ferromagnetic exchange ($J$ = +1.4 $cm^{-1}$) between Co(II) complex units. The role of O−H···O hydrogen bonds in mediating magnetic exchange is usually studied mostly for copper(II) complexes,[38] but there are also examples of iron(III) complexes, where magnetic exchange was found to be in the range from $J^{mag}$ = −0.52 $cm^{-1}$ to −1.05 $cm^{-1}$ ($J^{DFT}$ = −0.45 up to −0.86 $cm^{-1}$).[35d] Moreover, N−H···O and N−H···Cl hydrogen bonds were also found to propagate magnetic exchange between iron(III) atoms in the range from $J^{mag}$ = −0.20 $cm^{-1}$ to −0.40 $cm^{-1}$.[39] In our previous work,[35d] we also showed that magnetic exchange mediated by O−H···O hydrogen bonds in iron(III) and manganese(III) Schiff-base complexes correlates very well with the O···O distance and number of such hydrogen bonds connecting particular metal atoms. In the presented series, we can compare *J*-values for compound **3**, where there are intermolecular hydrogen bonds with $d$(O9···O2) = 2.580(3) Å and $J^{DFT}/J^{mag}$ = −0.53 $cm^{-1}$/−0.41(1) $cm^{-1}$, and compound **5** where the intramolecular hydrogen bond is present, with $d$(O3···O10) = 2.774(2) Å and $J^{DFT}$ = −0.45 $cm^{-1}$. Here, the *J*-values seem to correlate with O···O distance as well, as it was proposed in ref 35d.

Next, we focused on covalently mediated magnetic exchange in which Fe−O−Fe motif is present. The magnetostructural correlation for iron(III) $\mu$-O-bridged complexes was established by Gorund and Lippard[40] in the form of an exponential function as

$$J^{Lipp}\,[cm^{-1}] = -8.763 \times 10^{11} \exp(-12.663P) \quad (9)$$

where $P$ is a parameter that is defined as half of the shortest superexchange pathway between two iron(III)atoms. Recently, Vranovičová and Boča[41] have attempted to redo nonlinear regression using contemporary software as

$$J^{exp}\,[cm^{-1}] = -2.360 \times 10^{10} \exp(-10.661P) \quad (10)$$

and also to reformulate this magnetostructural correlation in the form of linear equations as

$$J^{\alpha}\,[cm^{-1}] = -3.98\alpha + 396 \quad (11)$$

or by

$$J^{P}\,[cm^{-1}] = 520.9P - 1047 \quad (12)$$

where $\alpha$ is the average value of Fe−O−Fe angle. In order to elucidate the applicability of such magnetostructural correlations, we compared *J* values for compounds **4** and **5** in Table 5. It is obvious that eq 12 incorrectly predicts the ferromagnetic exchange for two cases (Fe1···Fe2 in **4** and Fe2···Fe3 in **5**), and the values of the antiferromagnetic exchange for other bridges also are too high. However, eqs 10 and 11 seem to propose the sign of the *J* parameter correctly for all of the listed groups and, in some cases, deviations from the experimental values are even smaller than those in the case of utilizing eq 9. In our opinion, eqs 9 and 11 provided the most reasonable estimates of the isotropic exchange parameters and can be used for quick assessment/prediction of magnetic exchange based on simple X-ray parameters. Nonetheless, the DFT methods available nowadays to calculate the *J* parameters are superior to these general equations and can properly take into account all structural nuances of complexes influencing their magnetic properties, as manifested also in Scheme 2 for the family of iron(III) compounds reported herein.

**Scheme 2. Summary of Dominant Magnetic Superexchange Pathways in Compounds 1−5 Complemented by Comparison of *J* Values Derived from Analysis of the Experimental Magnetic Data, as Well as from DFT Calculations[a]**

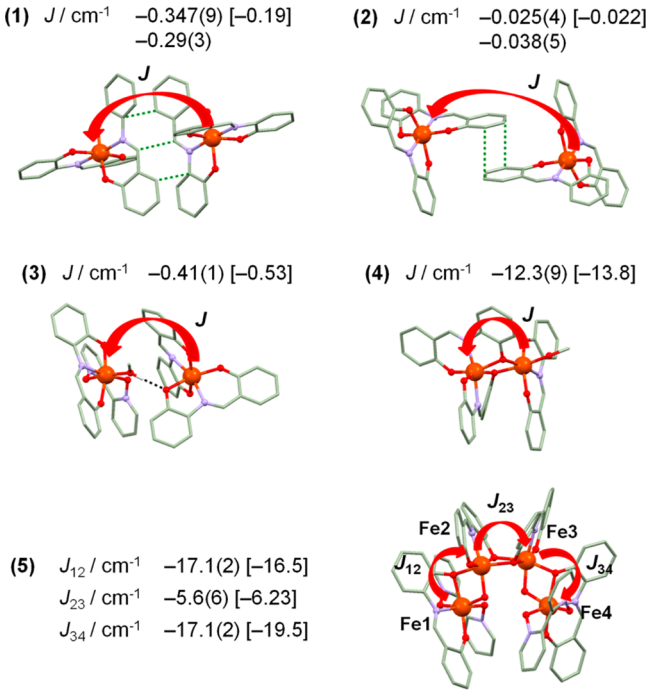


[a]DFT values are given in square brackets.

## CONCLUSIONS

To summarize, we have reported on the synthesis, X-ray structures, and evaluation of magnetic data of mononuclear, polymeric, and polynuclear iron(III) high-spin complexes $K[FeL_2]\cdot H_2O$ (**1**), $(Pr_3NH)[FeL_2]\cdot 2CH_3OH$ (**2**), $[FeL(bpyO_2)(CH_3OH)][FeL_2]\cdot CH_3OH$ (**3**), $[Fe_2L_3(CH_3OH)]\cdot 2CH_3OH\cdot H_2O$ (**4**), and $[\{Fe_2L_2\}(\mu\text{-}OH)_2\{FeL(bpyO_2)\}_2]$-



DOI: 10.1021/acs.inorgchem.5b01271
*Inorg. Chem.* 2015, 54, 8625−8638

$[BPh_4]_2 \cdot 2H_2O$ (**5**), utilizing the tridentate Schiff base ligand $H_2L$ ($H_2L$ = 2-hydroxyphenylsalicylaldimine). This family of iron(III) complexes gave us the opportunity to test/explore limits of theoretical methods and magnetochemistry with current scientific knowledge, which can be highlighted by comparing the theoretically predicted ($J^{DFT}$) and fitted ($J^{mag}$) values of the antiferromagnetic exchange parameters sorted by the increasing strength of the mediators as follows: $\pi-\pi$ stacking ($J^{DFT} = -0.022$ cm$^{-1}$/$J^{mag} = -0.025(4)$ cm$^{-1}$ in **2**) < C−H···O noncovalent contacts and $\pi-\pi$ stacking ($J^{DFT} = -0.19$ cm$^{-1}$/$J^{mag} = -0.347(9)$ cm$^{-1}$ in **1**) < O−H···O hydrogen bond ($J^{DFT} = -0.53$ cm$^{-1}$/$J^{mag} = -0.41(1)$ cm$^{-1}$ in **3**) < bis($\mu$-$O_{Ph}$) bridge ($J^{DFT} = -13.8$ cm$^{-1}$/$J^{mag} = -12.3(9)$ cm$^{-1}$ in **4**) < ($\mu$-$O_{Ph}$, $\mu$-OH) bridge ($J^{DFT} = -18.0$ cm$^{-1}$/$J^{mag} = -17.1(2)$ cm$^{-1}$ in **5**) (see Scheme 2). Thus, the main goal of the article has been fulfilled by findings that affordable theoretical methods are essential tools to explore magnetic interactions in the solid state mediated either by noncovalent or covalent interactions. There are several key points, which deserve to be stressed. First, the *ab initio* theoretical calculations at the DFT level of theory can reliably identify weak magnetic interaction through noncovalent contacts ($\pi-\pi$ stacking, C−H···O, and O−H···O hydrogen bonds, through a diamagnetic metal cation) in the crystal structures of the iron(III) coordination compounds, which is the crucial starting point to proper postulation of the final spin Hamiltonian. This puts more power in the hands of magnetochemists, who can analyze magnetic behavior more deeply, taking into account not only the temperature dependence of magnetization/susceptibility but also concurrently use field-dependent magnetization data measured at the lowest temperatures in fitting procedures. Furthermore, the predictive aspect of DFT calculations plays an indispensable role in proper assignment of magnetic exchange values in polynuclear systems, in which the number of possible superexchange pathways rapidly increases, along with the complexity of the system.

## ■ ASSOCIATED CONTENT

### Supporting Information

The Supporting Information is available free of charge on the ACS Publications website at DOI: 10.1021/acs.inorgchem.5b01271.

Additional tables and figures supporting DFT calculations (PDF)
CIF data for $C_{26}H_{20}FeKN_2O_5$ (CIF)
CIF data for $C_{35}H_{40}FeN_3O_4$ (CIF)
CIF data for $C_{51}H_{43}Fe_2N_5O_{10}$ (CIF)
CIF data for $C_{42}H_{41}Fe_2N_3O_{10}$ (CIF)
CIF data for $C_{120}H_{98}B_2Fe_4N_8O_{15}$ (CIF)

## ■ AUTHOR INFORMATION


### Corresponding Author

*Tel.: +420 585 634 352. Fax: +420 585 634 354. E-mail: zdenek.travnicek@upol.cz. Homepage: www.rcptm.com or http://agch.upol.cz/en/.


### Notes

The authors declare no competing financial interest.

## ■ ACKNOWLEDGMENTS

We acknowledge the financial support from the National Programme of Sustainability I (LO1305) of the Ministry of Education, Youth and Sports of the Czech Republic. We are also thankful to Dr. Milan Gembický and prof. Dr. Philip Coppens from Department of Chemistry at University at Buffalo for acquiring X-ray data of compound **5**.

## ■ REFERENCES


(1) (a) Kahn, O. *Molecular Magnetism*; VCH Publishers: New York, 1993. (b) Boča, R. *Theoretical Foundations of Molecular Magnetism*; Elsevier: Amsterdam, 1999.

(2) Boča, R. *Coord. Chem. Rev.* **2004**, *248*, 757−815.

(3) Bencini, A.; Gatteschi, D. *EPR of Exchange Couples Systems*; Springer−Verlag: Berlin, 1990.

(4) Boča, R.; Herchel, R. *Coord. Chem. Rev.* **2010**, *254*, 2973−3025.

(5) (a) Barra, A. L.; Debrunner, P.; Gatteschi, D.; Schulz, C. E.; Sessoli, R. *Europhys. Lett.* **1996**, *35*, 133−138. (b) Powell, G. W.; Lancashire, H. N.; Brechin, E. K.; Collison, D.; Heath, S. L.; Mallah, T.; Wernsdorfer, W. *Angew. Chem., Int. Ed.* **2004**, *43*, 5772−5775. (c) Ruiz, E.; Rodríguez-Fortea, A.; Cano, J.; Alvarez, S. *J. Phys. Chem. Solids* **2004**, *65*, 799−803. (d) Murugesu, M.; Clerac, R.; Wernsdorfer, W.; Anson, C. E.; Powell, A. K. *Angew. Chem., Int. Ed.* **2005**, *44*, 6678−6682. (e) van Slageren, J.; Rosa, P.; Caneschi, A.; Sessoli, R.; Casellas, H.; Rakitin, Y. V.; Cianchi, L.; Giallo, F. D.; Spina, G.; Bino, A.; Barra, A. L.; Guidi, T.; Carretta, S.; Caciuffo, R. *Phys. Rev. B* **2006**, *73*, 014422 10.1103/PhysRevB.73.014422. (f) Bagai, R.; Wernsdorfer, W.; Abboud, K. A.; Christou, G. *J. Am. Chem. Soc.* **2007**, *129*, 12918−12919. (g) Hoshino, N.; Ako, A. M.; Powell, A. K.; Oshio, H. *Inorg. Chem.* **2009**, *48*, 3396−3407. (h) Ako, A. M.; Mereacre, V.; Lan, Y. H.; Wernsdorfer, W.; Clerac, R.; Anson, C. E.; Powell, A. K. *Inorg. Chem.* **2010**, *49*, 1−3.

(6) See, e.g.: (a) Taft, K. L.; Delfs, C. D.; Papaefthymiou, G. C.; Foner, S.; Gatteschi, D.; Lippard, S. J. *J. Am. Chem. Soc.* **1994**, *116*, 823−832. (b) Guo, D.; McCusker, J. K. *Inorg. Chem.* **2007**, *46*, 3257−3274. (c) Albores, P.; Rentschler, E. *Inorg. Chem.* **2008**, *47*, 7960−7962. (d) Baran, P.; Boča, R.; Chakraborty, I.; Giapintzakis, J.; Herchel, R.; Huang, Q.; McGrady, J. E.; Raptis, R. G.; Sanakis, Y.; Simopoulos, A. *Inorg. Chem.* **2008**, *47*, 645−655. (e) Taguchi, T.; Stamatatos, T. C.; Abboud, K. A.; Jones, C. M.; Poole, K. M.; O'Brien, T. A.; Christou, G. *Inorg. Chem.* **2008**, *47*, 4095−4108.

(7) (a) Harvey, D. F.; Christmas, C. A.; McCusker, J. K.; Hagen, P. M.; Chadha, R. K.; Hendrickson, D. N. *Angew. Chem., Int. Ed. Engl.* **1991**, *30*, 598−600. (b) McCusker, J. K.; Christmas, C. A.; Hagen, P. M.; Chadha, R. K.; Harvey, D. F.; Hendrickson, D. N. *J. Am. Chem. Soc.* **1991**, *113*, 6114−6124. (c) Delfs, C.; Gatteschi, D.; Pardi, L.; Sessoli, R.; Wieghardt, K.; Hanke, D. *Inorg. Chem.* **1993**, *32*, 3099−3103. (d) Christmas, C. A.; Tsai, H. L.; Pardi, L.; Kesselman, J. M.; Gantzel, P. K.; Chadha, R. K.; Gatteschi, D.; Harvey, D. F.; Hendrickson, D. N. *J. Am. Chem. Soc.* **1993**, *115*, 12483−12490. (e) Powell, A. K.; Heath, S. L.; Gatteschi, D.; Pardi, L.; Sessoli, R.; Spina, G.; Delgiallo, F.; Pieralli, F. *J. Am. Chem. Soc.* **1995**, *117*, 2491−2502.

(8) (a) Spiro, T. G.; Saltman, P. *Struct. Bonding (Berlin, Ger.)* **1969**, *6*, 116−156. (b) Nordlund, P.; Eklund, H. *Curr. Opin. Struct. Biol.* **1995**, *5*, 758−766. (c) Rosenzweig, A. C.; Nordlund, P.; Takahara, P. M.; Frederick, C. A.; Lippard, S. J. *Chem. Biol.* **1995**, *2*, 409−418. (d) Logan, D. T.; Su, X. D.; Aberg, A.; Regnstrom, K.; Hajdu, J.; Eklund, H.; Nordlund, P. *Structure* **1996**, *4*, 1053−1064. (e) Que, L.; Ho, R. Y. N. *Chem. Rev.* **1996**, *96*, 2607−2624. (f) Kurtz, D. M., Jr. *JBIC, J. Biol. Inorg. Chem.* **1997**, *2*, 159−167.

(9) Neese, F. *Coord. Chem. Rev.* **2009**, *253*, 526−563.

(10) Elmali, A.; Elerman, Y.; Svoboda, I. *Z. Naturforsch., B: J. Chem. Sci.* **2001**, *56* (9), 897−900.

(11) CrysAlis CCD and CrysAlis RED, Version 1.171.33.52; Oxford Diffraction, Ltd.: Oxford, England, 2009.

(12) *APEX2, SMART-Plus and SADABS*; Bruker AXS, Inc.: Madison, WI, USA, 2004.

(13) Sheldrick, G. M. *Acta Crystallogr., Sect. A: Found. Crystallogr.* **2008**, *64*, 112−122.

(14) Neese, F. *WIREs Comput. Mol. Sci.* **2012**, *2*, 73−78.




DOI: 10.1021/acs.inorgchem.5b01271
*Inorg. Chem.* 2015, 54, 8625−8638

(15) (a) Lee, C.; Yang, W.; Parr, R. G. *Phys. Rev. B: Condens. Matter Mater. Phys.* **1988**, *37*, 785−789. (b) Becke, A. D. *J. Chem. Phys.* **1993**, *98*, 1372−1377. (c) Becke, A. D. *J. Chem. Phys.* **1993**, *98*, 5648−5652. (d) Stephens, P. J.; Devlin, F. J.; Chabalowski, C. F.; Frisch, M. J. *J. Phys. Chem.* **1994**, *98*, 11623−11627.
(16) (a) Ruiz, E.; Cano, J.; Alvarez, S.; Alemany, P. *J. Comput. Chem.* **1999**, *20*, 1391−1400. (b) Ruiz, E.; Rodríguez-Fortea, A.; Cano, J.; Alvarez, S.; Alemany, P. *J. Comput. Chem.* **2003**, *24*, 982−989.
(17) (a) Schafer, A.; Horn, H.; Ahlrichs, R. *J. Chem. Phys.* **1992**, *97*, 2571−2577. (b) Schafer, A.; Huber, C.; Ahlrichs, R. *J. Chem. Phys.* **1994**, *100*, 5829−5835. (c) Weigend, F.; Ahlrichs, R. *Phys. Chem. Chem. Phys.* **2005**, *7*, 3297−3305.
(18) (a) Neese, F.; Wennmohs, F.; Hansen, A.; Becker, U. *Chem. Phys.* **2009**, *356*, 98−109. (b) Izsak, R.; Neese, F. *J. Chem. Phys.* **2011**, *135*, 144105.
(19) (a) Grimme, S.; Antony, J.; Ehrlich, S.; Krieg, H. *J. Chem. Phys.* **2010**, *132*, 154104. (b) Grimme, S.; Ehrlich, S.; Goerigk, L. *J. Comput. Chem.* **2011**, *32*, 1456−1465.
(20) Momma, K.; Izumi, F. *J. Appl. Crystallogr.* **2011**, *44*, 1272−1276.
(21) Raptopoulou, C. P.; Boudalis, A. K.; Sanakis, Y.; Psycharis, V.; Clemente-Juan, J. M.; Fardis, M.; Diamantopoulos, G.; Papavassiliou, G. *Inorg. Chem.* **2006**, *45*, 2317−2326.
(22) (a) Oshio, H.; Hoshino, N.; Ito, T. *J. Am. Chem. Soc.* **2000**, *122*, 12602−12603. (b) Boskovic, C.; Rusanov, E.; Stoeckli-Evans, H.; Gudel, H. U. *Inorg. Chem. Commun.* **2002**, *5*, 881−886. (c) Boskovic, C.; Labat, G.; Neels, A.; Gudel, H. U. *Dalton Trans.* **2003**, 3671−3672. (d) Oshio, H.; Hoshino, N.; Ito, T.; Nakano, M.; Renz, F.; Gutlich, P. *Angew. Chem., Int. Ed.* **2003**, *42*, 223−225. (e) Boskovic, C.; Sieber, A.; Chaboussant, G.; Gudel, H. U.; Ensling, J.; Wernsdorfer, W.; Neels, A.; Labat, G.; Stoeckli-Evans, H.; Janssen, S. *Inorg. Chem.* **2004**, *43*, 5053−5068. (f) Oshio, H.; Hoshino, N.; Ito, T.; Nakano, M. *J. Am. Chem. Soc.* **2004**, *126*, 8805−8812. (g) Li, Y.; Wu, Q.; Lecren, L.; Clerac, R. *J. Mol. Struct.* **2008**, *890*, 339−345.
(23) Kopel, P.; Sindelar, Z.; Klicka, R. *Transition Met. Chem.* **1998**, *23*, 139−142.
(24) Reddy, K. R.; Rajasekharan, M. V.; Tuchagues, J. P. *Inorg. Chem.* **1998**, *37*, 5978−5982.
(25) (a) Trávnícek, Z.; Sindelár, Z.; Marek, J. *Z. Krist.−New Cryst. Struct.* **1997**, *212*, 125−126. (b) Nakamura, T.; Kuranuki, E.; Niwa, K.; Fujiwara, M.; Matsushita, T. *Chem. Lett.* **2000**, 248−249. (c) Bagherzadeh, M.; Tahsini, L.; Latifi, R.; Amani, V.; Ellern, A.; Woo, L. K. *Inorg. Chem. Commun.* **2009**, *12*, 476. (d) Nemec, I.; Machata, M.; Herchel, R.; Boča, R.; Trávníček, Z. *Dalton Trans.* **2012**, *41*, 14603−14610.
(26) (a) Dexin, L.; Xuegui, C.; Fangdong, G.; Fengling, L.; Qingchi, K. *Gaodeng Xuexiao Huaxue Xuebao* **1989**, *10*, 787. (b) Elmali, A.; Elerman, Y.; Svoboda, I.; Fuess, H. *Acta Crystallogr., Sect. C: Cryst. Struct. Commun.* **1993**, *49*, 965−967. (c) Elmali, A.; Elerman, Y.; Svoboda, I.; Fuess, H.; Griesar, K.; Haase, W. *Z. Naturforsch., B: J. Chem. Sci.* **1994**, *49*, 1239−1242. (d) Elmali, A.; Elerman, Y.; Svoboda, I.; Fuess, H.; Griesar, K.; Haase, W. *Z. Naturforsch., B: J. Chem. Sci.* **1994**, *49*, 365−369. (e) Elmali, A.; Elerman, Y.; Svoboda, I.; Fuess, H. *J. Mol. Struct.* **2000**, *516*, 43−47. (f) Elmali, A.; Elerman, Y.; Svoboda, I. *Z. Naturforsch., B: J. Chem. Sci.* **2001**, *56*, 897−900. (g) Elmali, A.; Elerman, Y.; Zeyrek, C. T.; Svoboda, I. *Z. Naturforsch., B* **2003**, *58*, 433−437.
(27) Man, W. L.; Xiang, J.; Lau, P. H.; Gao, S.; Wong, W. T.; Lau, T. C. *Sci. China: Chem.* **2010**, *53*, 2106−2111.
(28) Mondal, K. C.; Kostakis, G. E.; Lan, Y. H.; Wernsdorfer, W.; Anson, C. E.; Powell, A. K. *Inorg. Chem.* **2011**, *50*, 11604−11611.
(29) Ke, H. S.; Zhao, L.; Guo, Y.; Tang, J. K. *Inorg. Chem.* **2012**, *51*, 2699−2705.
(30) (a) The distortion parameter is defined as the sum of deviations from 90° of the twelve *cis* angles in the coordination sphere. (b) Guionneau, P.; Marchivie, M.; Bravic, G.; Létard, J.-F.; Chasseau, D. *Top. Curr. Chem.* **2004**, *234*, 97−128.
(31) (a) Maurice, R.; Graaf, C. d.; Guihery, N. *Phys. Chem. Chem. Phys.* **2013**, *15*, 18784−18804. (b) Malrieu, J. P.; Caballol, R.; Calzado, C. J.; de Graaf, C.; Guihéry, N. *Chem. Rev.* **2014**, *114*, 429−492.
(32) Cramer, C. J.; Truhlar, D. G. *Phys. Chem. Chem. Phys.* **2009**, *11*, 10757−10816.
(33) Ruiz, E. *Struct. Bonding (Berlin, Ger.)* **2004**, *113*, 71−102.
(34) The standard deviations were calculated as $\sigma_i = (P_{ii}^{-1} \cdot S/(N-k))^{-1/2}$, where $P_{ij} = \sum(\delta\mu_n/\delta a_i \cdot \delta\mu_n/\delta a_j)$ and $S = \sum(\mu_n - \mu_n^{exp})^2$ with $n$ = 1 to $N$; $a_i$ and $a_j$ are fitted parameters, $N$ is number of experimental points (sum of temperature and field dependent data), $\mu_n$ and $\mu_n^{exp}$ are the calculated and experimental effective magnetic moments for given temperature and magnetic field. The $\sigma_i$ was then multiplied by $t_{95\%}$ (Student's *t*-test) to provide confidence limits with 95% probabilities listed in the text.
(35) (a) Herchel, R.; Pavelek, L.; Trávníček, Z. *Dalton Trans.* **2011**, *40*, 11896−11903. (b) Šalitroš, I.; Boča, R.; Herchel, R.; Moncol, J.; Nemec, I.; Ruben, M.; Renz, F. *Inorg. Chem.* **2012**, *51*, 12755−12767. (c) Nemec, I.; Zoufalý, P.; Herchel, R.; Trávníček, Z. *Inorg. Chem. Commun.* **2013**, *35*, 50−53. (d) Nemec, I.; Herchel, R.; Šilha, T.; Trávníček, Z. *Dalton Trans.* **2014**, *43*, 15602−15616.
(36) Bandeira, N. A. G.; Maynau, D.; Robert, V.; Le Guennic, B. *Inorg. Chem.* **2013**, *52*, 7980−7986.
(37) Rajnák, C.; Titiš, J.; Fuhr, O.; Ruben, M.; Boča, R. *Inorg. Chem.* **2014**, *53*, 8200−8202.
(38) see e.g. (a) Desplanches, C.; Ruiz, E.; Rodríguez-Fortea, A.; Alvarez, S. *J. Am. Chem. Soc.* **2002**, *124*, 5197−5205. (b) Guennic, B. L.; Amor, N. B.; Maynau, D.; Robert, V. *J. Chem. Theory Comput.* **2009**, *5*, 1506−1510. (c) Bandeira, N. A. G.; Guennic, B. L. *J. Phys. Chem. A* **2012**, *116*, 3465−3473.
(39) Atzori, M.; Sessini, E.; Artizzu, F.; Pilia, L.; Serpe, A.; Gómez-García, C. J.; Giménez-Saiz, C.; Deplano, P.; Mercuri, M. L. *Inorg. Chem.* **2012**, *51*, 5360−5367.
(40) Gorun, S. M.; Lippard, S. J. *Inorg. Chem.* **1991**, *30*, 1625−1630.
(41) Vranovičová, B.; Boča, R. *Nova Biotechnol. Chim.* **2013**, *12*, 70−74 10.2478/nbec-2013-0008.


DOI: 10.1021/acs.inorgchem.5b01271
*Inorg. Chem.* 2015, 54, 8625−8638